Drug Coating & Release from CNT-Forests grown on Biodegradable Stainless-Steel Alloy Stent

A thesis submitted to McGill University in partial fulfillment of the requirements of the degree of
Masters of Experimental Surgery

Department of Experimental Surgery

April 2020

Supervisor: Dr. Renzo Cecere

Co-Supervisor: Professor Rosaire Mongrain

Co-Supervisor: Professor Jean-Luc Meunier

Submitted by: Samer Alroujayee

Table of Contents

LIST OF FIGURES

List of Tables

Acknowledgment:

I would like to give special thanks and express my sincere gratitude to Dr.Cecere and his Cardiac Surgery team, Professor Mongrain and his Mechanical Engineering team and last but not least Professor Meunier and his Chemical Engineering team including Dr. Kaustubh Basu. I also would like to thank Professor Mongeau and his team for sharing their tools and equipment to facilitate the completion of this project.

Also, very special thanks to Eng. Aqeel Alrebah from the Chemical Engineering lab, who played huge role in achieving these results by providing extra facilities and tools such as the scanning electron microscopy and the UV-Vis.

Abstract:

According to the American Heart Association, heart diseases are the leading cause of death in the U.S, where roughly 610,000 people die every year due to cardiac disease. Coronary heart disease is the most common heart disease, with approximately 400,000 dying annually in the United States. Therefore, endovascular stents play a major role in the treatment of the coronary heart disease. However, the use of permanent metallic stents can generate major complications such as subacute thrombosis and in-stent restenosis. This reason is why multiple solutions have been evaluated and studied in the recent years to replace the permanent metallic stents. One of these possible alternatives is "Biodegradable Stents" mainly made of polymer, zinc and magnesium. Nonetheless, scientists still must test the mechanical and biocompatibility properties of the biodegradable stents. Dr.Cecere and his team have successfully identified suitable alternative to the existing biodegradable materials (polymer, magnesium and zinc). For instance, iron and stainless-steel based stents are very safe to use, as these materials have always been used in medical implants. The key objective of this project is that the chemical vapor deposition techniques will allow producing a series of carbon nanotubes on the surface of the new biodegradable materials (iron & stainless) to be used as a drug carrier to allow for control release of the medical compound by modifying the structure of the carbon nanotubes features and allow for biodegradation.

Resume

Selon l'American Heart Association, les maladies cardiaques sont la principale cause de décès aux États-Unis, où environ 610 000 personnes meurent chaque année des suites d'une maladie cardiaque. La maladie coronarienne est la maladie cardiaque la plus courante, où environ 400 000 personnes meurent chaque année aux États-Unis. Par conséquent, les stents endovasculaires jouent un rôle majeur dans le traitement de la maladie coronarienne. Cependant, l'utilisation de stents métalliques permanents peut entraîner des complications majeures telles que la thrombose subaiguë et la resténose intra-stent. C'est la raison pour laquelle plusieurs solutions ont été évaluées et étudiées ces dernières années pour remplacer les stents métalliques permanents. L'une de ces alternatives possibles consiste en des «stents biodégradables» principalement en polymère, zinc et magnésium. Néanmoins, les scientifiques doivent encore tester les propriétés mécaniques et de biocompatibilité des stents biodégradables. Dr.Cecere et son équipe ont identifié avec succès une alternative appropriée aux matériaux biodégradables existants (polymère, magnésium et zinc). Par exemple, les stents à base de fer et d'acier inoxydable sont très sûrs à utiliser, car ces matériaux ont toujours été utilisés dans les implants médicaux. L'objectif principal de ce projet est que les techniques de dépôt chimique en phase vapeur permettront de produire une série de nanotubes de carbone à la surface des nouveaux matériaux biodégradables (fer & inox), a utiliser comme support de médicament pour permettre contrôler la libération du composé médical en modifiant la structure des caractéristiques des nanotubes de carbone et permettre la biodégradation.

Chapter 1: Introduction

1.1 Motivation

Cardiovascular diseases (CVD) have been major cause of death globally for long time. For instance, in the U.S , there is an average of 790,000 heart attacks and strokes annually [1], which creates heavy burden on the healthcare system with estimated cost of $89 billion in 2016, and this figure is estimated to jump to $ 215 billion in 2035 [1]. Despite the fact the treatments of cardiovascular diseases have advanced a lot in the last 10 years, yet we observe an increase in the cardio vascular diseases due to several factors such as obesity, smoking habits, aging….etc. [1]. According to the World Health Organization, approximately 17.6 million people died of CVD in 2012, which represents 31.3% of global mortality. However, in 1977 the world witnessed the first breakthrough in the treatment of CVD when Andreas Roland Grüntzig performed the first balloon angioplasty.

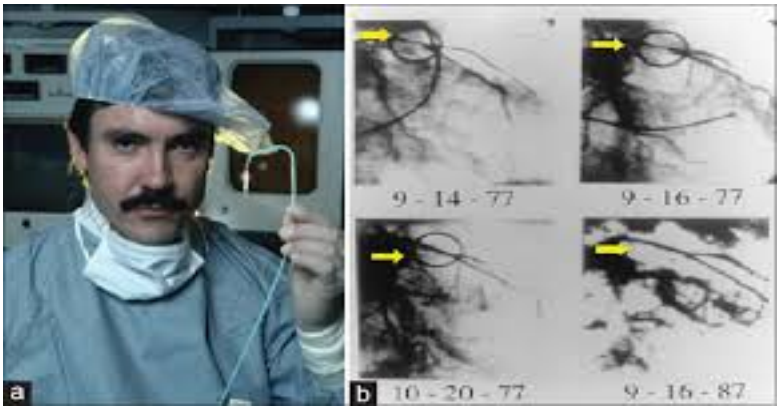

Figure 0-1: First angioplasty operation performed by Dr.Gruntzig [2]

Angioplasty is also known as Percutaneous Coronary Intervention, and is used to open the clogged heart artery by inserting and inflating a balloon to remove the plaque and install a metallic stent to widen and keep the artery open [3]. However, there were two major complications: Thrombosis and acute occlusion, where 5-10% of patients suffered from this

immediately after the operation, on the other hand 30% of the patients suffered from late restenosis in the first six months. There were also many complications such as bleeding at the insertion site, infection, and ruptured artery etc. [3].

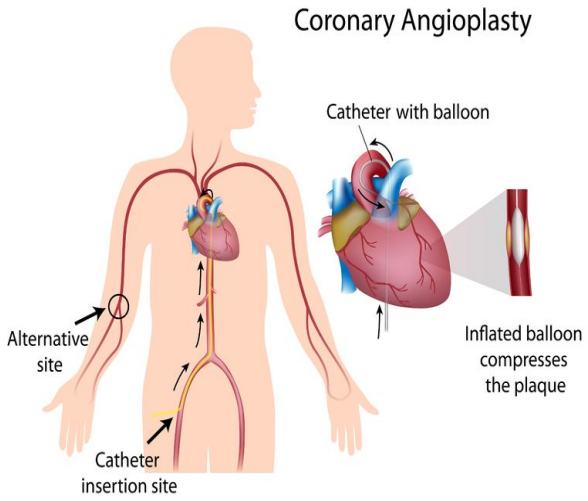

Figure 1-2: Angioplasty procedures [2]

Therefore, to solve the problem of elastic recoil, the first generation of bare-metal stent (BMS) was developed, with the first BMS being was approved by the FDA in the late 80's. However, the issue of late in-stent restenosis continued at the rate of 20-30% [1].

1.2 Research Objectives

The Main objective of this thesis is to grow CNTs on SS mesh (substrate A) using method described in (Prof. Meunier's article) and adapt modifications to see the possibility of growing CNTs on a (Fe 80%/316L SS 20%), Substrate B.

Also, the second main objective was to test the efficacy of CNTs coating with methylene blue, MB, (simulating drug) and its release in water-glycerol solution (simulating blood's viscosity).

The secondary objectives are:

1. To qualitatively investigate the adsorption of MB on CNTs by a dipping method
2. To quantitatively study the MB release at various time intervals

3. To investigate the influence of varying the environment conditions of MB release (i.e. static vs in-motion solution) to simulate the blood flow.

1.3 Thesis Overview

Chapter 2 provides background information and literature review of the biodegradable stents and cardiovascular disease required to understand the clinical condition of interest and heart failure. Chapter 3 describes the methods used for the design and production of carbon nanotubes concept and the materials/equipment required to characterize through numerical and in-vitro experiments, and also in chapter 3 we discuss the results at the end. Chapter 4 discusses the conclusion; limitations details the contribution to the field and provides a list of tasks suggested for future work.

Chapter 2: Literature Review

2.1 Materials of Biodegradable Stents

The main objective from designing and implementing the biodegradable stent is the same for the permanent metallic stent, with the exception that the biodegradable stent will simply disappear within specific time frame after implementation. This is to avoid the common complications created by the permanent stent such as late in-stent restenosis and thrombosis. Therefore, biodegradable stents should still meet the same strength and flexibility requirements as the permanent stent [4]. Below are short descriptions of the most common biodegradable stents being studied:

2.2.1 Magnesium Based-Stent

Magnesium is a lightweight metal, and it has the necessary mechanical properties similar to the natural bone such as high ductility and strength levels. Additionally, it is completely safe as it is essential element in the body, where it is absorbed and digested by the human body. In Figure 2-1 below, it is an example of magnesium-based stent from Biotronik:

Figure 2-1: Magnesium Stent [2]

That's why Magnesium is already used in medical implants such as orthopedics implants due to its high strength property. Magnesium also has the property of not interfering with radiological examinations including MRI [4]. However, the key challenge with magnesium is that its biodegradation rate is typically too fast. Therefore the challenge for magnesium based or any other type of stents is to find the right balance between degradation time and radial strength [5].

2.2.2 Polylactic Stents

PLLA (poly-l-lactide) is a polymer that is widely used in fabricating biodegradable stents due to its high melting point and low solubility [4, 6]. Also, it is already used in many medical

implants, and the degradation rate can be easily more controlled compared to magnesium. In Figure 2-2, we see samples of polymer-based stents.

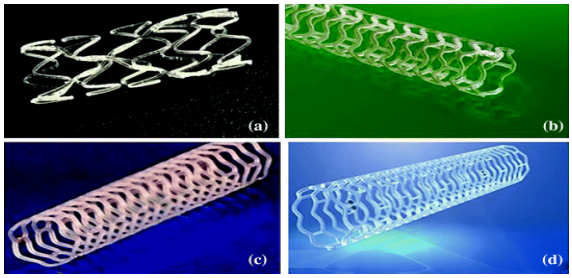

Figure 2-2: Various biodegradable stents made of polymer [2]

However, the downside of the Polymers in general is that it does not have the necessary radial strength like the other biodegradable metals [4] [6]. Biodegradable polymers are fabricated by fermentation from starchy materials and sugars. Also, the melting point for these polymers is very high (175 degree), and polymeric stents are typically transparent and easily produced[7]. These kinds of polymers exist in several forms such as, poly(L-lactide), poly(D-lactide), poly(DL-lactide) L-PLA and D-PLA have high tensile strength and low elongation[7], they are also semi-crystalline. On the other hand, Dl-lactide is very amorphous. There are several biodegradation factors that influence the behaviors of these polymers such as[7], molecular weight and molecular weight distribution, melting temperature, crystal structure, modulus of elasticity, surface area, and hydrophobic properties.

2.3 Current Challenges of Biodegradable Stents

2.3.1 Injury and Inflammations

The procedure of implementation of the biodegradable stent can still cause chronic inflammation and cell proliferation. This is why many researchers are considering the creation of Drug-Eluting Biodegradable Stent as shown on Figure 2-3 which will carry anti-inflammatory drugs [8]. These would carry anti-inflammatory drugs and allow a slow controlled release of these drugs [8]. This thesis looks at a specific structure bounded to the stents that would allow such slow controlled release of drugs.

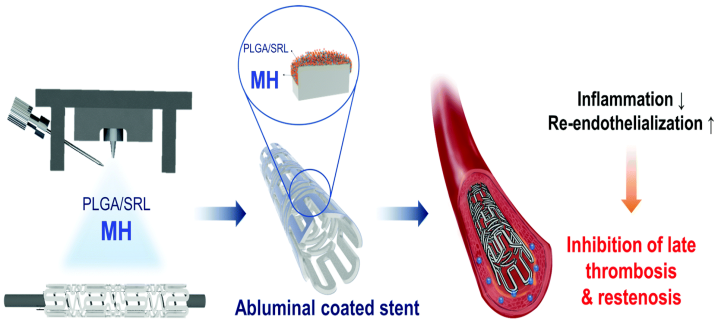

Figure 2-3: : Process of drug releasing by DES [2]

2.3.2 Shear Stress and Endothelial Function

Vascular shear stress can cause atherosclerotic disease and it can affect the healing after the stent implementation [4, 9]. The majority of the current biodegradable stents have bulky struts and huge shape which could injure the lumen wall easily, which leads to endothelial dysfunction (ED) [10]. Endothelial dysfunction could also affect the coronary circulation (Figure 2-4) and not only the stented area [4]. Therefore, the strut size and shape need to evolve towards much smaller sizes than the current bulky structures, but yet keeping the same strength strenght properties.

2.3.3 Stent Thrombosis

Recent researches and medical studies have proven in many cases that there is a high risk of stent thrombosis especially within 1 year of the stent placement [4]. Once again, the main obstacle in the design of the biodegradable stent is that to reach sufficient radial strength, the size of the strut has to be large which will lead to larger lumen coverage and create more blood flow obstruction[4, 10]. Currently, there are many studies about the use of Mg-based stents as an ideal alternative. The Magnesium has higher level of radial strength than polymer, with smaller strut design [8]. Magnesium strut surface is extremely smooth which will minimize the lumen wall injuries [4]. Below is the summary of the require essential characteristics and properties for the ideal biodegradable stent, the current challenges of the materials and design and the possible solutions.

2.4 Current Biodegradable Stents

2.4.1 Igaki-Tamai Stent

In the late 80s, Kyoto Medical company in Japan developed the first biodegradable stent and named it after Dr. Hideo Tamai as recognition for his involvement in this project (Figure 1-7) [11]. It was non-drug eluting stent made of PLLA (Poly-lactic acid). In Figure 2-4 below, we see a sample of 1st generation of Igaki-Tamai stent.

Figure 2-4: : 1st biodegradable stent developed by Igaki-Tamai Stent [11]

Its strut thickness was 170 μm. For the delivery and placement procedures, eight French catheters were used. The initial studies included 15 patients for 6 months, and 25 stents were implemented. There was no major complication reported within the first month. The TLR (Target Lesion Revascularization) was 10.5% after 6 months [4, 11]. In 2010, the company conducted another extensive study of 10 years follow up, which included 50 patients and 84 stents placements. There were two complications of thrombosis reported. Survival rates after 10 years were as the following, for all-cause death 87%, cardiac death 98%, major adverse Cardiac Events 50%, while the TLR rates were 16% after 1 year, TLR rates were 22% after 5 years, TLR rates were 38% after 10 years [12]. Despite the positive results of Igaki-Tamai stent, there were still few challenges such as the requirement of the use of eight French guiding catheter and the need to heat the contrast agent.

2.4.2 Absorb BVS

Abbot Vascular, the multi-national medical company launched its first biodegradable drug-eluting stent Absorb 1 (Figure 2-5), which was an everolimus eluting bioresorbable vascular scaffold [4, 13]. The Absorb 1 had a strut thickness of 150 μm, and it was made of polymer (PLLA).

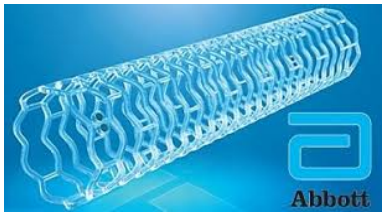

Figure 2-5: Abbott 1st generation Biodegradable Stent [2]

The results from their initial studies which included 30 patients were as the following [4, 14], success rate was 94%, 12 months MACE rate was 3.3%, 5 years MACE 3.4%, 1 patient suffered from TLR after 46 days, area stenosis was 31.6%-33.3% between 18 months and 5 years, scaffold shrinkage from 6.94+-1.47 to 6.29+-1.70mm [14]. Later on, ABBOTT developed another generation of biodegradable drug eluting stent (Absorb BVS 1.1), made of polymer (PLLA) coated with PDLA (Poly-D-L-Lactic) [4]. The strut thickness was 150 μm but with new modifications in the design to increase radial and mechanical strength. Abbott conducted 3 year follow up studies which included 250 patients and concluded the following results [15], MACE rate was 9%, mean lumen area changed from 7.23+-1.24 to 5.99+-1.61 mm after 2 years, TLR was 4%, Thrombus was 0.8%.

2.4.3 D-esolve

Elixir Medical Corporation developed its first polymer biodegradable drug-eluting stent (myolimus-eluting stent), Figure 2-6 which was mainly made of PLLA with strut thickness of 150 μm and degradation time frame of 12 months [4].

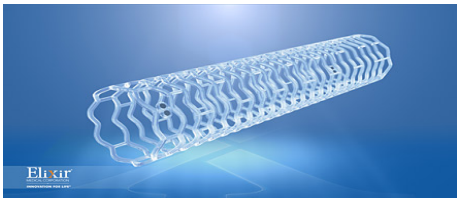

Figure 2-6: Elixir 1st generation biodegradable stent [2]

Elixir Medical Corporation conducted the initial human experiments on 16 patients with 15 successful operations [4]. The results from their first studies are, Lumen loss was .19mm, 1 TLR, 3 MACE, no thrombosis. Later one, Elixir Medical developed a 2nd generation of fully

biodegradable drug eluting stent (DESolve NX) with the same strut thickness as the first generation 150 μm, but with different anti-inflammatory drug (novolimus) [4]. The company conducted a second multi-center study on 126 patients and follow up of 6 months. The results were [4], implantations rate was 97%, MACE was 7.4%, 1 death due to thrombosis, TLR was 4.1%. Elixir is currently testing a 3rd generation of their biodegradable stent with smaller strut structure of 100 μm [4].

2.4.4 REVA

Reva Medical launched their first biodegradable drug eluting stent ReZolve made of PTD-PC (minothryrosine polycarbonate) with strut thickness of 115-230 μm, and the drug was sirolimus [4].

Figure 2-7: : Reva's 1st generation biodegradable stent [2]

One of the key advantages of the new generation is the fact that it was visible in X-Ray images. Reva conducted their first medical researches including 50 patients, the results were, lumen loss was .29mm+-.33mm after 12 months, device technical success was 85%. The key difference of Reva stent was the thinner strut thickness 115 μm [4].

2.4.5 AMS

Biotronik Germany, developed the first metallic biodegradable stent, which was not a drug-eluting stent (Figure 2-8)

Figure 2-8: : Biotronik, Germany 1st stent [2]

It was mainly made of magnesium with strut thickness of 165 μm [4, 16]. The results from their initial studies on 63 patients with follow up of 12 months were [17], MACE rate was 26.7%, no death, no thrombosis, TLR was 45% after 12 months. Later on, Biotronik developed a 2nd generation to control the degradation rate and increase the mechanical strength by launching DREAMS with strut thickness of 125 μm, and it was coated with polymer (PLGA). It was also a drug eluting stent (paclitaxel) [4]. Based on their studies on 46 patients, the success rate was 100% over 12 months without any death nor thrombosis [4, 18].

2.4.6 XINSORB

Shanghai Biotechnology developed their first-generation stent made of polymer (PLLA) and coated with sirolimus drug [4]. 80% of the drug degraded within 30 days, and the strut thickness was 150 μm [19]. The 1st Xinsorb stent was implanted in 2013 [20] after conducting their first in human clinical trials, the results were [4, 20], success rate was 100%, no MACE, no stent thrombosis, lumen loss was .18+-.21 mm. In summary section 1.5 below provides two tables showing the comparative characteristic of the various biodegradable stents, Table (1-1) and the results of clinical trials (Table 1-2).

2.5 Summary of Stents Characteristics and Clinical Trials

The most common polymer used in the fabrication of the biodegradable polymer-based stent is poly-L-lactic acid (PLLA). PLLA has a tensile modulus that 100-fold less that stainless steel. In other words to maintain the necessary radial strength as the metallic stents, the polymer based stents need to have thicker struts by approximately 240% [21]

Scaffold	Strut material	Coating material	Eluted drug	Strut Thickness (μm)	Time (months)	Current status
Igaki-Tami	PLLA	None	None	170	24-36	CE mark
Absorb BVS 1.0	PLLA	PDLLA	Everolimus	156	18-24	Discontinued
Absorb BVS 1.1	PLLA	PDLLA	Everolimus	156	24-48	CE mark
Absorb BVS-New generation	PLLA	PDLLA	Everolimus	<100	NA	NA
DeSolve	PLLA	None	Myolimus	150	12-24	CE mark
REVA	PTD-PC	None	None	200	24	Discontinued
AMS-1	PLLA	None	None	170	24-36	CE mark
Xinsorb	PLLA	PDLLA	Sirolimus	160	24-36	Clinical trial

Table 2-1: Summary of biodegradable stents

Stent	Trial	Material	Drugs	Patients	LLL(mm)	TLF(%)	MACE (%)	ST(%)
Absorb 1.0	Absorb A	PLLA	Everolimus	30	.44+-.35	NA	3.3	0
Absorb 1.1	Absorb B1/B2	PLLA	Everolimus	101	.27+-.32	NA	6.9	0
DESolve	DESolve Nx	PLLA	Novolimus	126	NA	5.7	5.7	.8
AMS-I	AMS	Magnesium	Paclitaxel	63	1.08+-.49	26.7	26.7	0
Dreams	Biosolve	Magnesium	Sirolimus	46	.52+-.39	7	2.3	0
Xience	Meta-analysis	CoCr	Everolimus	1225	.10+.24	5.2	3	.6

Table 2-2: Summary of trials from 1 year follow up with biodegradable stents, LLL (late lumen loss), TLF (target lesion failure), MACE (major adverse cardiac event), ST (Stent thrombosis)

2.6 Summary of Mechanical Behavior of Polymer-based Stents

Below is a summary of the mechanical and physical properties of several biodegradable components used in the design and fabrication of bioresorbable materials:

Polymer	Modulus	Strength	Elongation @ break %	Degradation (months)
PLA	2-4	65	2-6	18-30
PDLLA	1-3.5	40	1-2	3-4
PLLA	2-4	60-70	2-6	>24
PGA	6-7	90-110	1-2	4-6
Mg (alloy)	40-50	220-330	2-20	3-12
SS 316L	193	668	40	Biostable

Table 2-3: Mechanical and physical properties of biodegradable materials (PLA, polylactic acid, PDLLA, poly-DL-lactic acid, PLLA, poly-l-lactic acid, PGA, polyglycolide, Mg magnesium, SS stainless steel) [21]

PLLA polymer has higher tensile strength and modulus of elasticity than other polymers and slower absorption time than other polymers, which makes it the best option for BDS. However,

PLLA has limited expansion and can fracture due to over dilation [21], leading to limited radial strength. The absorption of the PLLA happens in three steps, hydrolysis, that affects the mechanical properties of the polymer-based stents. In this phase the molecular weight decreases affecting the mechanical performance causing a reduction in crystallinity [21], a decrease in mechanical strength occurs because of the scission of the amorphous tie chains linking crystalline regions, The proposed new coating with carbon nanotube would avoid the problems observed with the degradation of current coatings (flaking, particles embolization) because of their nano size. In addition, the carbon nanotubes coating provides a new means for

drug carrying by varying its characteristics (density, length and resulting entanglement) which allows for controlling the drug release kinetics.

2.7 Summary of Stent Coatings

In stent restenosis is still a critical problem, this is why it became necessary to solve this issue by modifying the material of the stent material and changing the external layer of the stent surface in order to enable the stent to perform anticoagulant and antiplatelet therapies to inhibit neointimal growth. Therefore, coating specific materials to the surface of the stent, is a very practical method to change the surface properties of the stent, and to improve its biocompatibility and hemocompatibility to avoid thrombosis and restenosis [22, 23]. There are three major types of stent coatings (biocompatible coatings, drug-delivery coatings and polymer-free coatings). For the first generation of metal base stent, the metallic surface always released ions after deployment which caused inflammation. Thus, the researchers and developers added stent coating to the metal base stent to prevent any ion release upon implantation. This kind of stent coating played the role as a barrier to ion release [22, 23], but it was not capable to carry or deliver any drug which can be necessary for intima proliferation in case of artery injury during angioplasty procedures. Once again, researchers had to find another solution by developing a biocompatible polymer coating with the capacity of drug carrying to store and elute pharmaceutical agents to the lesion site. However, patients with polymer-based coatings suffered from higher percentage of thrombosis. Recently, scientists started exploring nanotechnology to develop polymer-free stent coatings. With nanotechnology researchers would change the pore, the particle, and the thickness of the stent surface at the nanoscale [22, 23].

2.7.1 Gold Coating

Gold-coated stents produced less macroscopic and histopathologic changes in the aorta, is radiopaque material and it is coated to stainless steel stents to increase fluoroscopic visibility. However, there were major complications caused by the use of gold-coating such as higher neointimal hyperplasia cases.

2.7.2 Polymer Coating

Polymers consist of large molecular compounds made of repeated structural units. They have good capacity of carrying and delivering therapeutic agents to injured tissues in the arteries. They are divided into two types (non-degradable and biodegradable).

a) Non-Degradable Polymers

The current drug eluting stents are coated with nonbiodegradable polymers such as ethylene-co-vinyl acetate and styrene-b-isobutylene-b-styrene. Nonbiodegradable polymers have demonstrated that they can reduce restenosis in comparison to bare metal stents. However, it was observed that an increase in the rate of mortality after 18 months to 3 years after the use of this kind of coatings was observed [23].

b) Biodegradable Polymers

Poly (lactic acid) (PLA), poly(glycolic acid) and poly(lactic-co-glycolic acid) (PLGA) are the most common used biodegradable polymers. They are easily degraded and metabolized by the body. Despite the huge potential of the biodegradable polymers, there are still key challenges with the degradation rate. Degradation is affected by various factors such as pH, polymer size, and molecular weight, which makes the drug release more difficult to control [23].

Chapter 3: Project (Methods & Results)

3.1 Project / Objectives

The Main objective of this thesis is to grow CNTs on SS mesh (substrate A) using method described in (Prof. Meunier's article) and adapt modifications to see the possibility of growing CNTs on a (Fe 80%/316L SS 20%), Substrate B. Also, the second main objective was to test the efficacy of CNTs coating with methylene blue, MB, (simulating drug) and its release in water-glycerol solution (simulating blood's viscosity). The secondary objectives are, to qualitatively investigate the adsorption of MB on CNTs by a dipping method, to quantitatively study the MB release at various time intervals and to investigate the influence of varying the environment conditions of MB release (i.e. static vs in-motion solution) to simulate the blood flow.

3.2 Carbon Nanotubes Growth Experiments

3.2.1 Experimental Procedures: CNTs Growth

The substrate used for the production of CNTs on stainless steel (SS), was 316SS mesh, where the samples were sonicated in acetone for 10-15 minutes for cleaning purposes. Following the cleaning phase with sonication, the samples are dried in the furnace for 15-25 minutes at 30-45 degree to be prepared for the CNT growth in the furnace using the chemical vapor deposition (CVD) method. CVD is a used to fabricate high quality and high performance carbon nanotubes, where the substrate is inserted in the middle of the furnace and then exposed to high temperature after the injection of carbon source gases such as acetylene which produces the CNTs on the surface of the substrate in a specific time.

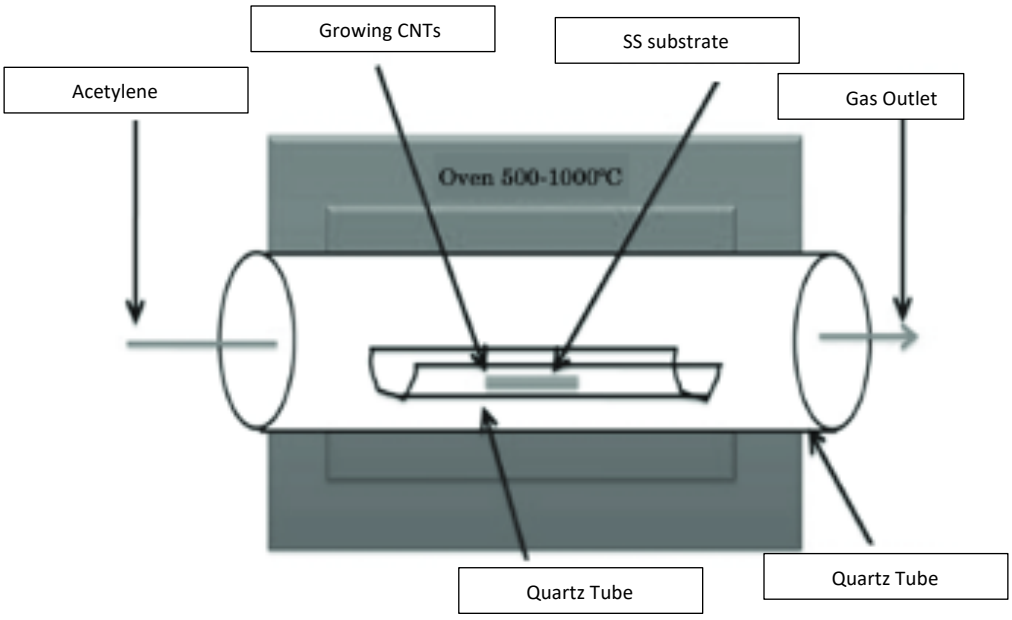

Figure 3-1: Chemical Vapor Deposition Furnace (CVD) [24]

3.2.2 Experiment Set up: CNTs Growth

After the cleaning and the preparation of the stainless steel (SS) samples, we start the set up for the Thermo Fischer furnace as per the figures 3-2, and 3-3 below:

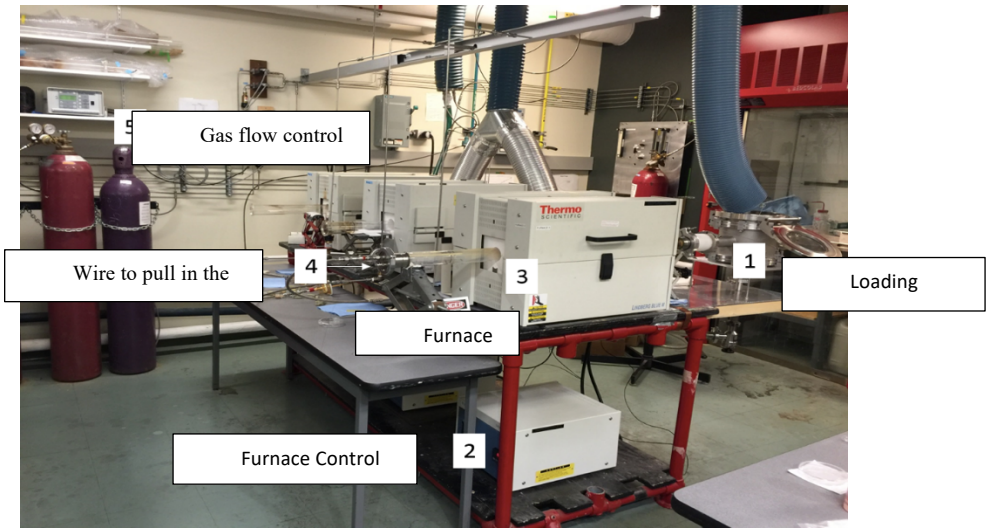

Figure 3-2: Thermo-Fischer CVD Furnace [25]

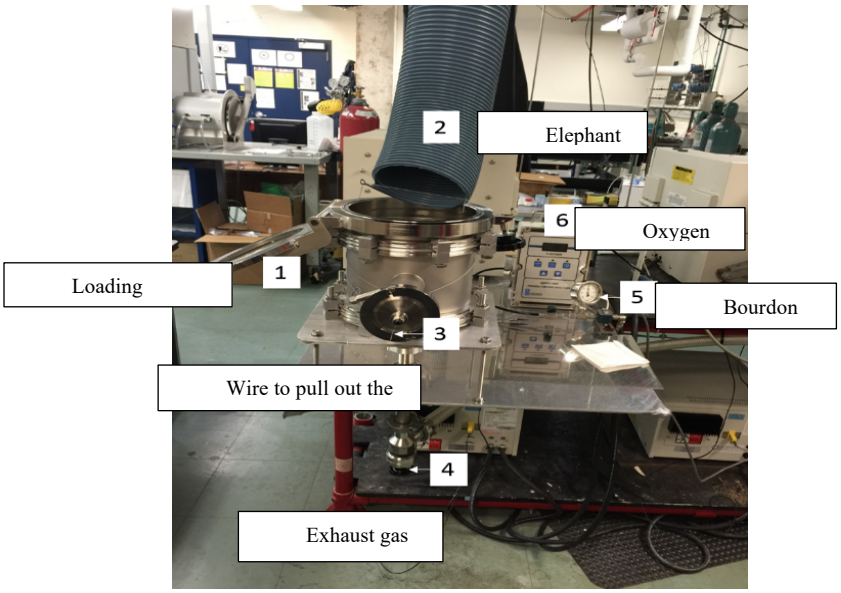

Figure 3-3 : CVD Set-up at Chemical Lab [25]

We initially set up the temperature up to 700 degree and wait for 15-20 minutes before the placement of the SS samples. For the SS samples, there is no need for etching neither for pre-heat treatment unlike with the other Fe-SS samples. Because Fe-SS sample has chromium on its surface which prevents the growth of carbon nanotubes, that's why it is necessary to do etching and pre-heat treatment for the Fe-SS before the growth phase. Then, once the temperature reaches 700 degree and after 15 minutes for the temperature to stabilize. Once the temperature is stabilized, the samples are put on a ceramic boat and then the boat is positioned in the middle of the furnace, then the loading chamber is closed and any oxygen and any other gas are purged by the use of argon for 10 minutes at 1500 sccm. Then the flow rate of the argon is reduced to 592 sccm, and then the acetylene at 68 sccm is injected for 5 minutes. This phase is called the growth phase, where the CNTs are produced by the injection of acetylene, while exposed to 700 degree. Then, after 5 minutes the acetylene is closed, while the argon is opened at 592 sccm for 30 minutes. After 30 minutes, the argon line is closed, and then wait for 2 minutes before the loading chamber is opened. Once the reactor is opened, the gas evacuation horn is placed to the loading chamber to remove any remaining gas from the furnace. Then, we the samples are pulled out and then the reactor is sealed again. Finally, the reactor is sealed, and the argon source is opened at the flow of 592 sccm, then the furnace is set to RES (reset) mode until the temperatures reaches 200 degree. After that, the reactor is set to RUN mode to burn all the remaining carbon in the furnace. This is the protocol for the production of CNTs on SS samples only. However, in the case of the Fe-SS samples, the following steps are needed with minor

modification of the above protocol: after the cleaning of the samples with the sonication method, the Fe-SS samples are placed in acid (HCI 37%) under the fume hood for 10-15 minutes. Then the samples are washed with distilled water, then the samples are dried in the fume hood for 30-60 minutes, then the pre-heat treatment procedures begin, where the samples inside the furnace are exposed to 850 degree for 30 minutes. The reason, this is done is to remove the chromium layer which is on the top of the surface of the Fe-SS substrate. This layer prevents the growth of the CNTs; therefore, the etching is for 10-15 minutes then the samples are exposed to high temperature for 30 minutes to simply create a suitable catalyst for the growth of CNTs later on during the growth phase. The pre-heat treatment is as per figure 3-4 below:

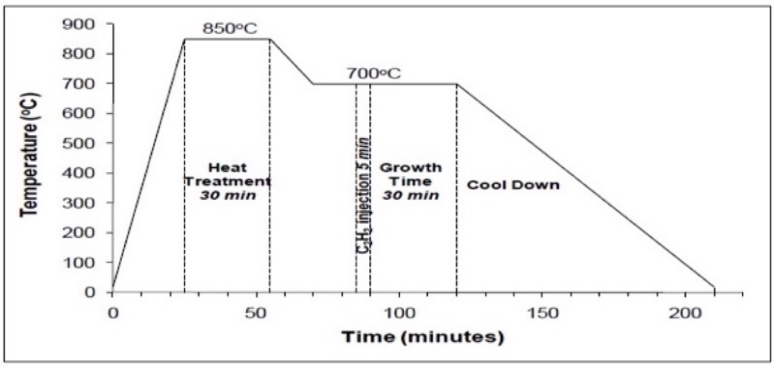

Figure 3-4 Pre-heat Treatment Process [25]

3.2.3 Experiment, CNTs Growth on Stainless Steel Mesh / SS-Grid

There were over 8 experiments conducted to grow the CNTs on the surface of the Stainless-Steel mesh. The same protocol is followed of the SS mentioned above; however, minor changes are done with the flow rate and time of the acetylene to optimize the best production of the CNTs.

	Argon		Acetylene		Argon		Sample Weight (g)		
sample	Flow rate (sccm)	Purging time (min)	Flow rate (sccm)	Growth Time (min)	Flow rate (sccm)	Purging time (min)	Before CNT growth	After CNT growth	carbon loading (g)
1	592	15	45	5	1000	15	0.0718	0.0731	0.018
2	592	5	22,5	5	1000	15	0.0515	0.0522	0.013
3	592	5	68	5	1000	15	0.0708	0.0712	0.005
4	592	5	68	2	1000	15	0.0544	0.0553	0.016
5	592	5	45	5	1000	15	0.0997	0.1018	0.021
6	592	5	45	5	1000	15	0.0568	0.058	0.021
7	592	5	45	5	1000	15	0.054	0.0555	0.027
8	592	5	45	5	1000	15	0.0598	0.0604	0.010

Table 3-1: Protocols of CNTs growth procedures for SS samples

For each experiment, the weight was measured and after of the sample to perform analysis quantitively, in addition to the visual and SEM analysis.

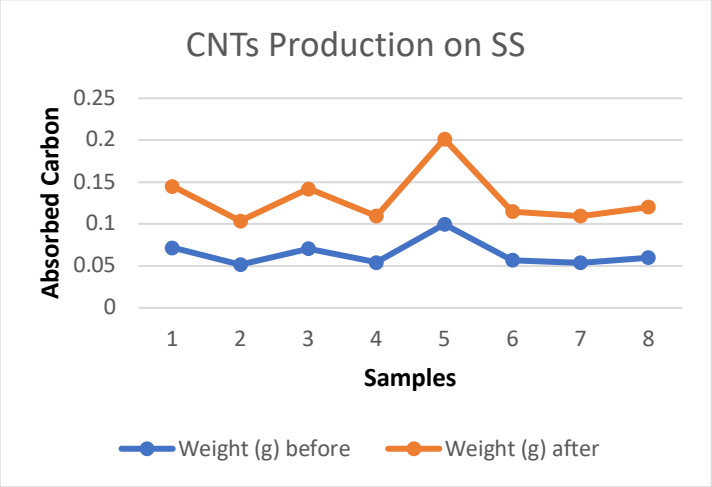

Figure 3-5: Comparison of SS samples' weight before and after CNTs growth

Based on the measurements above giving the weights before and after, it was concluded that there was always an increase in the weight which means that there was a carbon absorption that leads to the growth of CNTs. Therefore, it was clear that we had the best results were obtained for the samples 6 and 7 protocols as per Table 3-2:

Samples	Argon (sccm)	Argon (min)	Acetylene @ flow rate of 45 sccm	Argon(sccm)	Argon (min)2	Weight (g) Before	Weight (g) After	Absorbed Carbon 9g)
6	592	5	5 min	1000	15	0.0568	0.058	0.021
7	592	5	5 min	1000	15	0.054	0.0555	0.027

Table 3-2: Best results of CNTs growth for SS experiments

The largest difference in carbon content observed corresponded to the protocol of samples 6 and 7. However, all CNT growth protocols used gave carbon loading differences within 0.01g. It was also conducted an initial visual observation, where the dark black color means that the carbon has been absorbed by the mesh and there are CNTs on the surface in comparison with grey color before the CVD experiment.

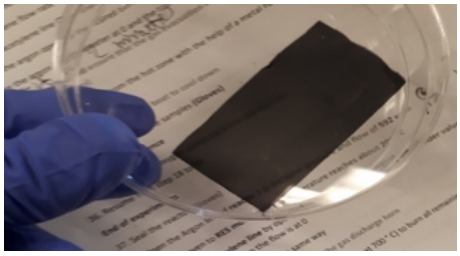

Figure 3-6: Image of SS sample after growth of CNTs

Later, SEM analysis were performed at different scale to confirm the production of CNTs on the SS-grid. The results were good using Meunier's et al, CNTs protocol with C_2H_2 (Acetylene) flow rate at 45 sccm and growth time of 5 minutes as we clearly see the CNTs on the surface of the SS-grid as per the images in Figure 3-7 below:

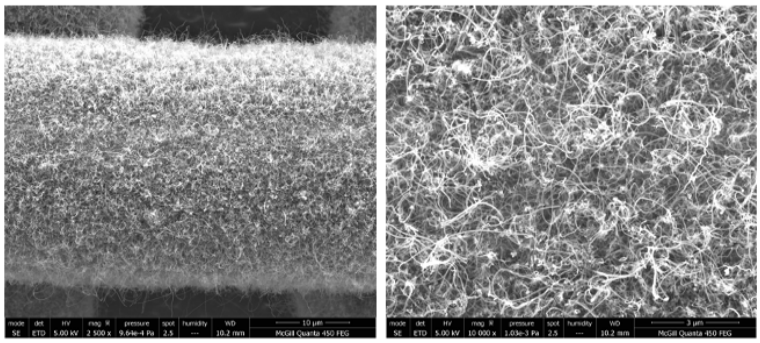

Figure 3-7: SEM images of SS-grid with 5 minutes growth and Acetylene injection at 45 sccm

For the other the samples with C_2H_2 injection rate of 68 sccm, and growth time for 2 minutes, the SS-grid was mostly covered with amorphous carbon, with partial CNT coverage as per the SEM image in Figure 3-8 below:

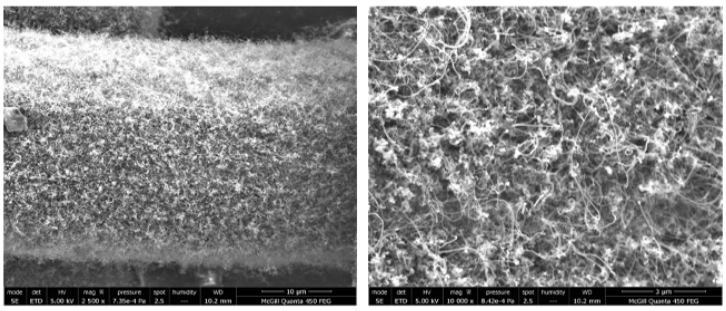

Figure 3-8: SEM Image of SS-grid with 2 minutes growth and Acetylene injection at 68 sccm

3.2.4 CNTs Growth on Fe-SS substrate without pre-Heat Treatment and without etching

Following the same CNTs protocol for stainless steel on the alloy from Frattolin et al. was not very successful for our first attempt to grow CNTs on Fe-SS sample, as only partial growth was obtained of CNTs but not as homogenous growth as per the image 3-9, and 3-10 below:

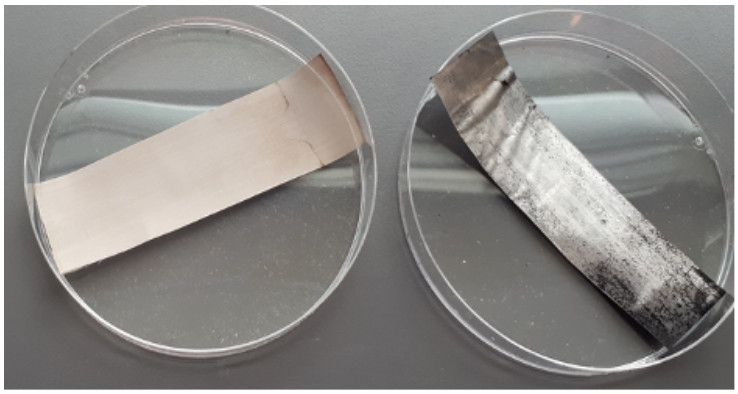

Figure 3-9: Original protocol for CNT growth on SS mesh not successful for Mongrain's alloy (left image Fe-SS before growth, right image Fe-SS after growth)

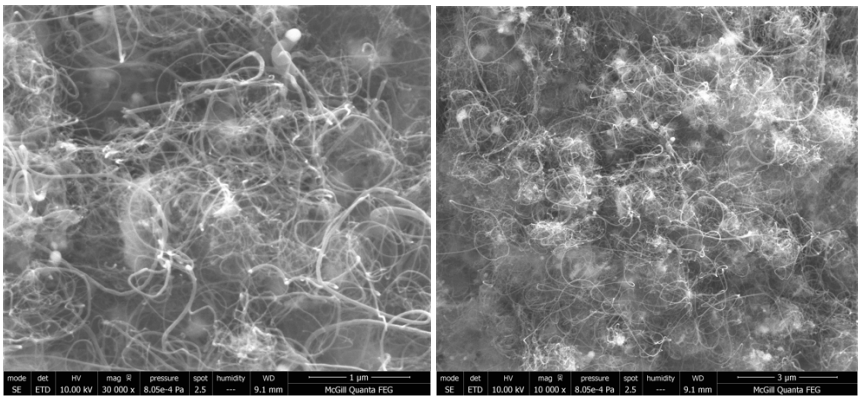

Figure 3-10: SEM images of Fe-SS substrate with 5 minutes growth and Acetylene injection at 45 sccm without any etching or pre-heat treatment

From the previous images in Figures (3-9, 3-10), we clearly see that there was partial growth of CNTs on the edges of the Fe-SS substrate, but it was not homogenous growth. That's it was decided to add certain modifications to the original SS-grid protocol such as etching with 37% HCl, pre heat treatment for 30 minutes and also reduce the size of the sample to have higher concentration of acetylene on the substrate.

3.2.5 CNTs Growth on Fe-SS Substrate with pre-Heat Treatment (Temperature at 750 degree) & Etching

For the 3rd experiment, different etching time 3, 5,7 and 10 minutes were performed. The pre-heating temperature was changed to 750 degree, while the rest of the sittings were fixed such as the acetylene time of 10 minutes and the pre-heat treatment for 30 minutes as per the protocol in the Table 3-3 below:

Samples	Etching time (minutes)	Argon time 1st Part	Acet @ 68 sccm	Argon Time 2nd Part	Pre- Heating	Weight before etching (g)	Weight After Etching (g)	Weight After Growth (g)	Carbon Absorbed (g)
1	3	5	10 min	15	30 min @ 750	0.1755	0.1701	0.226	0.0559
2	5	5	10 min	15	30 min @ 750	0.1491	0.1421	0.219	0.0769
3	7	5	10 min	15	30 min @ 750	0.1652	0.1612	0.2134	0.0522
4	10	5	10 min	15	30 min @ 750	0.1673	0.1634	0.254	0.0906

Table 3-3: Protocols of CNTs growth for Fe-SS (2nd Experiment)

As per the analysis above, the best growth was obtained at etching time of 10 minutes based on the measured carbon absorbed which was 0.0906 g. A scanning electron microscopy (SEM) analysis was done and no CNTs were observed. Instead amorphous carbon was produced as per the images in Figure 3-11 below:

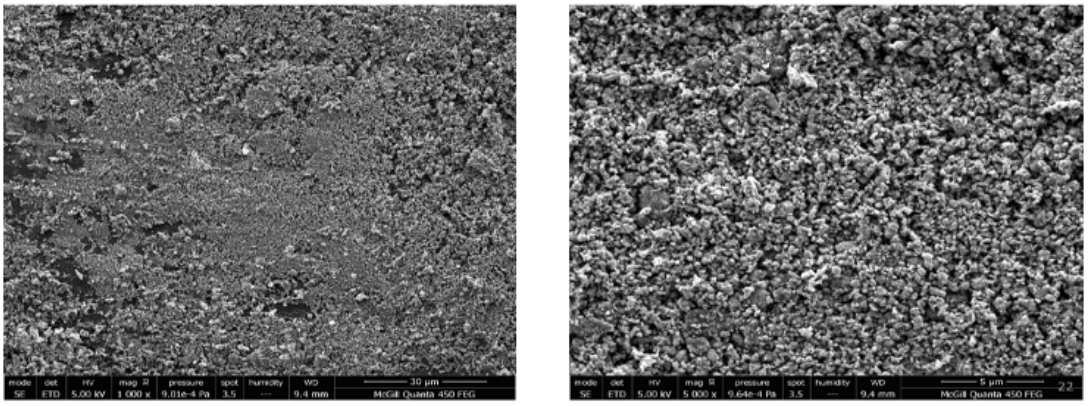

Figure 3-11: At pre-heating temperature 750 °C after etching for 10 minutes and at 10 minutes of acetylene injection, CNTs did not form

3.2.6 CNTs Growth on Fe-SS substrate with pre-Heat Treatment (Temperature at 800 degree) & Etching

For the Fe-SS sample which is made of 80% iron and 20% Stainless steel, a similar protocol was followed as the SS mesh, however with major modification such as the etching with acid and pre-heat treatment of 30 minutes at a temperature of 800 degree as per the protocol in Table 3-4 below:

Samples	Etching time (min)	Pre-heating time (min) @ 800 C	Argon purging time (min)	Acet. Time (min) @ 45 sccm	Argon purging time (min)	Sample weight before etching (g)	Sample weight After Etching (g)	Sample weight After CNT growth (g)	Difference
1	**15**	**30**	5	15	15	0.7253	0.7199	0.7245	0.0046
2	**15**	**30**	5	10	15	0.6105	0.6084	0.618	0.0096
3	**15**	**30**	5	7	15	0.5213	0.5121	0.5201	0.008
4	**15**	**30**	5	5	15	0.6232	0.6201	0.6243	0.0042

Table 3-4: CNTs growth procedures for Fe-SS samples with etching for 15 minutes & pre heat treatment at 800 degree

Based on the analysis above, it was concluded that the best growth was obtained when the etching for 15 minutes was done, the acetylene injection for 10 minutes, and pre-heat treatment at 800 degree for 30 minutes.

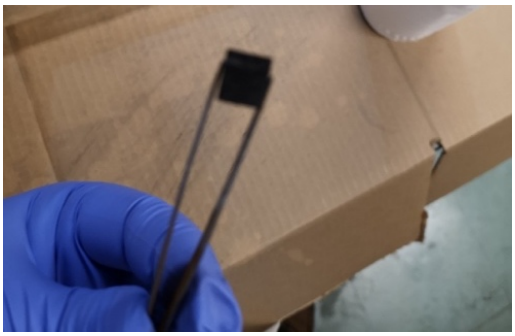

Figure 3-12: Image of Fe-SS sample after the growth of CNTs, with etching for 15 minutes and 10 minutes of acetylene injection

It was conducted scanning electron microscopy analysis for the Fe-SS substrate and the results were very good, where a homogenous growth was seen as per the SEM images in Figure 3-13 below:

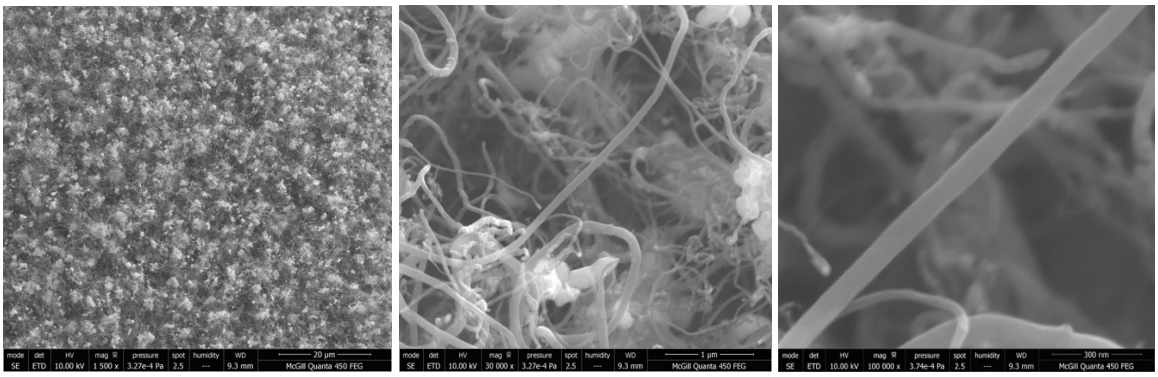

Figure 3-13: Image of SEM for the FE-SS substrate with CNTs, with etching for 15 minutes and 10 minutes of acetylene injection

In summary from these 4 experiments, that for a stainless-steel mesh (SS-Grid), it is clear that the CNT's protocol from Meunier et al. needs to be followed, which includes acetylene injection for 5 minutes at flow rate of 45 sccm. For other protocols such as acetylene injection for 2 minutes at flow rate of 68 sccm, some growth could be possible, but it will not be homogenous or efficient. On the other hand, the (Fe80-SS20) alloy had little growth of CNTs by following the regular CNTs protocol of SS-grid, but the growth will not homogenous and it will be only partial. Therefore, to have a homogenous and concentrated CNTs growth for Fe-SS sample, we need to etch the Fe-SS substrate for 10-15 minutes, and pre-heat treat it for 30 minutes at 800 degree. When we tried to etch it for less than 10 minutes and pre heat treat it for 750 degree, we ended up with amorphous carbon as shown earlier.

3.3 Drug Capture in CNT Forest for Slow Delivery

Carbon nanotubes CNTs are made of carbon and formed in cylindrical shape with diameter in nanometer scale and length in few microns to few millimeters [26], because of their shape and mechanical properties, which allows to form mesh structures. They are being studied to be used in pharmaceutical and biomedical applications as drug carriers. Multi forest carbon nanotubes (MFCNTs) have high surface area and high capacity of adsorbing with many drugs such as anti-inflammation agents [26]. MFCNTs have proven their efficacy in drug delivery directly into cells and keeping the drug attached without metabolism during delivery inside the human body [26-28]. Many researches also have proven that when attached to carbon nanotubes, the molecules are delivered more effectively and safely into cells than by conventional methods [26, 29-31]. That is why in this project, we have decided to create CNTs on the surface of Fe-SS alloy using McGill's CNTs protocol, to be used as drug carrier.

3.3.1 Experimental procedure: Drug Coating/Release

For the drug coating by dipping method, we will conduct several experiments to establish proof of concept. The first trial will be with concentrated MB on CNTs for SS-grid, next we conduct another trial with concentrated MB on CNTs for Fe80-SS20 substrate, then another experiment with diluted MB on CNTs for SS-grid and finally another trial with diluted MB on CNTs for Fe80-SS20. This phase will be to establish proof of concept for the drug dip coating for both substrates (SS-grid & Fe-SS). Then the next phase will be testing the drug release for CNTs on (Fe80-SS20) alloy with different time intervals for both static condition (no blood flow) and dynamic condition (by fluid motion). For each experiment, we will use the UV-vis

technique from the company Spectrology/Flame-CHEM-VIS, to measure the light intensity and correlate it with the MB concentrations volume. We measured the intensity of the solution by UV-vis before and after the dip coating to determine if there is any adsorption of the dye molecules by the carbon nanotubes. Where we put the solution in the sample cuvette, and then we transmit a light with certain intensity through the solution, then the attenuated light is received by the detector on the other side and the intensity of the received light is measured. If we have an increase in the intensity, then we know that an adsorption happened, and if there is a decrease in the intensity of the liquid then we know that there was a release of the drug or dye particles from the CNTs. We will establish two reference curves, where the first curve is with the use of distilled water and for the second reference curve, it will be with the use of 37% glycerin mixed with water to simulate the viscosity of the blood.

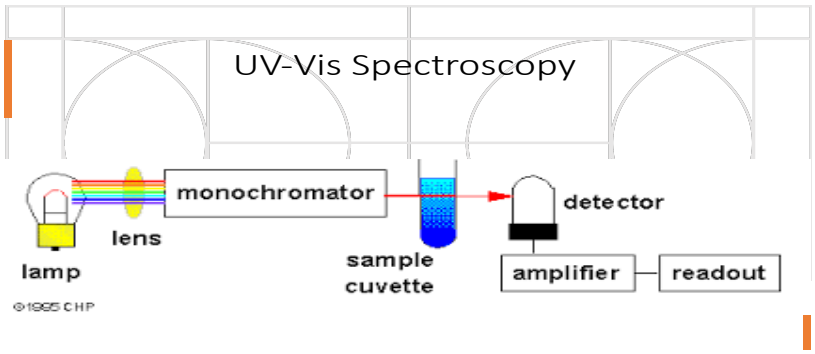

Figure 3-14: UV-vis Mechanism Ultraviolet–visible spectroscopy or ultraviolet–visible spectrophotometry refers to absorption spectroscopy or reflectance spectroscopy in part of the ultraviolet and the full, adjacent visible spectral regions. [32]

Figure 3-15: Image of Dip Coating (left image in static phase, right image in dynamic condition)

After the synthesis of the multi carbon nanotubes forest on both the stainless-steel grid and the Fe80-SS20 substrate, the next phase of the project will be testing the coating capacity of the CNTs of the methylene blue. We decided to use MB for this project because it is both a medication and a dye. The scientific name for it is **methylthioninium chloride.** Our initial objective was to check if the CNTs on both the SS-grid and Fe80-SS20 will attract any MB molecules to it, and would we be able to control the release of the dye molecules later on. Therefore, we designed this phase into these key parts, initial testing of dye adsorption for the SS-grid and Fe80-SS20 samples by the use of dip coating method, drug coating for all SS-grid and Fe80-SS20 samples in multiple time range from 5 minutes all the way to 3 hours, drug release for all SS-grid and Fe80-SS20 samples in both static and motion. The dip coating method consists of three major steps as per Figure 3-16:

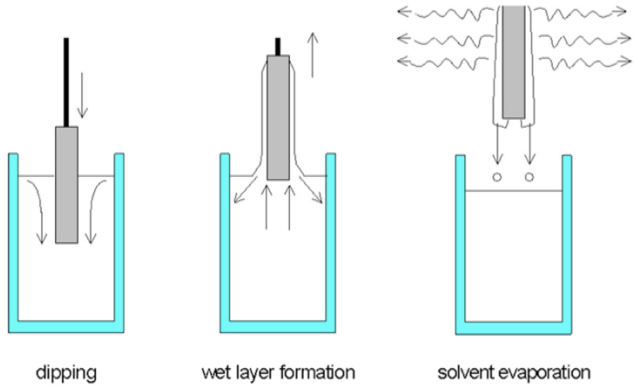

Figure 3-16: Absorption Process [8]

First of all, we mix distilled water with certain quantity of the dye, then dip the sample into the solution for certain time, then finally we take out the sample and dry it for certain time before the release phase experiment.

3.3.2 CNTs coating with concentrated MB - (Stainless-Steel Grid)

After the initial dip coating trial for the SS-grid, with concentrated MB dye as per the image 4-17 below, we performed the scanning electron microscopy images to analyze whether there has been any drug coating to the carbon nanotubes forest on the SS-grid as per Figures (3-18,3-19):

1st SS sample @

10 minutes dipping

2nd SS sample @

15 minutes dipping

Figure 3-17: Image of SS-grids in coating dip phase in concentrated MB

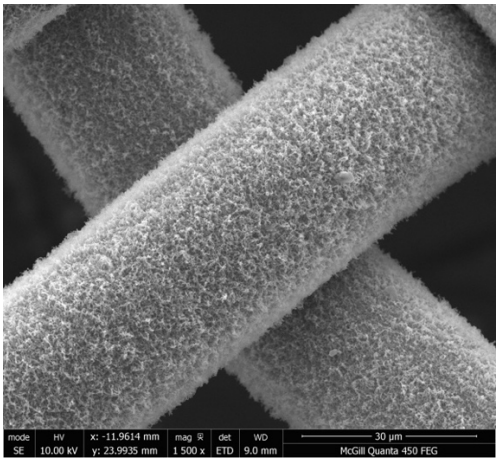

Figure 3-18: SEM image of SS-Grid before dip coating for 15 minutes

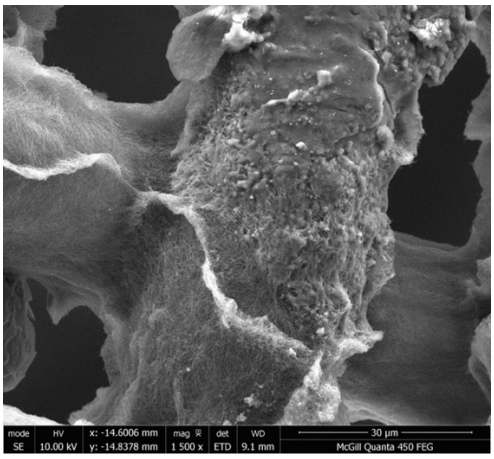

Figure 3-19: SEM image of SS-grid after dip coating for 15 minutes

When we compare the two images in Figure 3-18 & 3-19, we clearly see the MB molecules attached to the CNTs on the surface of the SS-grid as in Figure 3-19.

3.3.4 CNTs coating with concentrated MB (Fe-SS)

After the second dip coating trial for the Fe-SS substrate, with concentrated MB dye as per Figure 4-20, we performed the scanning electron microscopy images to analyze whether there has been any drug coating to the carbon nanotubes forest on the Fe-SS substrate as per the images in Figures (3-21,3-22) below:

1st Fe-SS sample

@ 10 minutes dipping

2nd Fe-SS sample

@ 15 minutes dipping

Figure 3-20: Image of SS-grids in coating dip phase in concentrated MB for 10-15 minutes

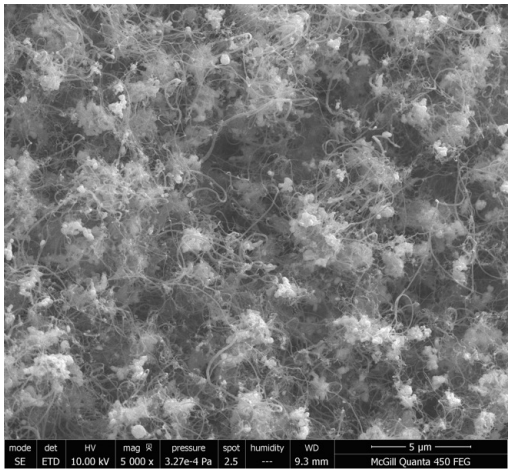

Figure 3-21: SEM image of Fe-SS substrate before dip coating, (Fe80-SS20) for 15 minutes of coating in concentrated MB

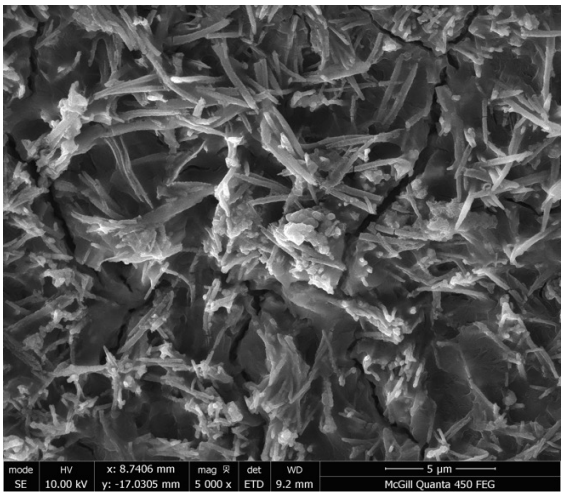

Figure 3-22: SEM image of Fe-SS substrate after dip coating, Fe80-SS20 for 15 minutes of dipping in concentrated MB

From the images above, we see a direct comparison before and after dip coating for a Fe-SS substrate with CNTs. We clearly see that the multi forest carbon nanotubes on the surface of Fe-SS substrate are well coated with MB molecules.

3.3.5 Experiment of SS-Grid with CNTs coating with diluted MB

Once again, we could establish the conclusion that there was some color release by the CNTs on the SS-Grid once put in distilled water as per Figure 3-23.

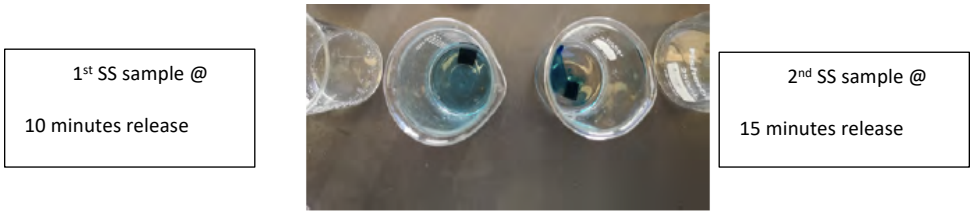

Figure 3-23: effect of the dipping time could effectively be observed visually upon MB removal in water over 10 minutes & 15 minutes

Based on the results above, we did more specific trials based on the coating time and based on the dye concentration level. The first experiment was on SS-Grid with dip coating time of 3 hours as per Table 3-5 below:

SS Samples	Coating Time	Vol BM (in 100mL dist. water)	Intensity before adsorption	Intensity After adsorption	Difference
1	3 hours	0.0 ml	2092.29	2092.29	0
2	3 hours	0.5 ml	1550.17	1568	17.83
3	3 hours	1.0 ml	1295.91	1315.84	19.93
4	3 hours	1.5 ml	1059.94	1102.05	42.11

← Increasing

Table 3-5: Intensity increases during coating phase

After conducting the dip coating trial for 3 hours based on the following concentrations of MB volume, 0 ml, 0.5 ml, 1 ml, 1.5ml. We measured the intensity of the solution by UV-vis before and after the dip coating to determine if there was any adsorption of the dye molecules by the carbon nanotubes. The results during the desorption phase indicate an increase in intensity of the MB dye in water as a result of a release of the adsorbed dye, which means in other words that the CNTs attracted many molecules of the dye, where we see an increase in the intensity after the dip coating, which confirms that the CNTs has carried MB molecules.

3.3.6 Experiment of Fe-SS with CNTs / CNTs coating with diluted MB

The first experiment was to assess visually the absorption capacity by the new CNTs created on the Fe-SS samples. We used 20 ml of distilled water, 0.5 ml of Methylene Blue dye, and the coating time was 2 hours. The initial results of the preliminary test clearly showed that MB was absorbed on the CNT forest following a single dip coating sequence as per the Figure 3-24 below:

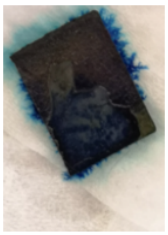

Figure 3-24: Release phase of FE-SS after dip coating sequence

The Fe-SS started releasing the MB as soon as it was put in the distilled water, also we could see that clearly on the image, when the sample was put on a white tissue, it left traces of blue

color. We also conducted a similar experiment for the SS-grid, where the SS-grid were dipped for different time range from 30 minutes to 2 hours.

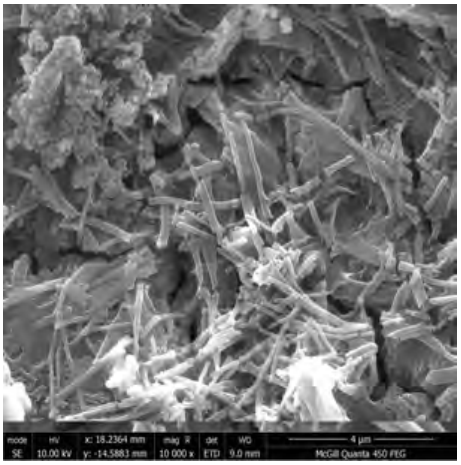

Figure 3-25: SEM image of SS-grid after dip coating for 2 hours in diluted MB

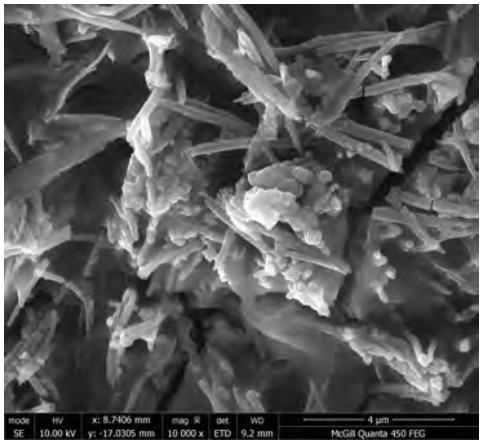

Figure 3-26: SEM image of Fe-SS substrate after dip coating for 2 hours in diluted MB

Figure 3-25 & Figure 3-26 above demonstrate a comparison between stainless steel mesh with CNTs and Fe-SS with CNTs after dip coating. We could clearly see the similarity of the structure on both surfaces.

3.4 Establishing 1st Reference Curve

In order to generate a reference curve on MB concentration in water, we fixed the coating volume at 0.3 micro liter. Then, we took intensity measurements of the light transmitted in order to generate a relationship between the change of intensity in relation with the intensity and concentration level.

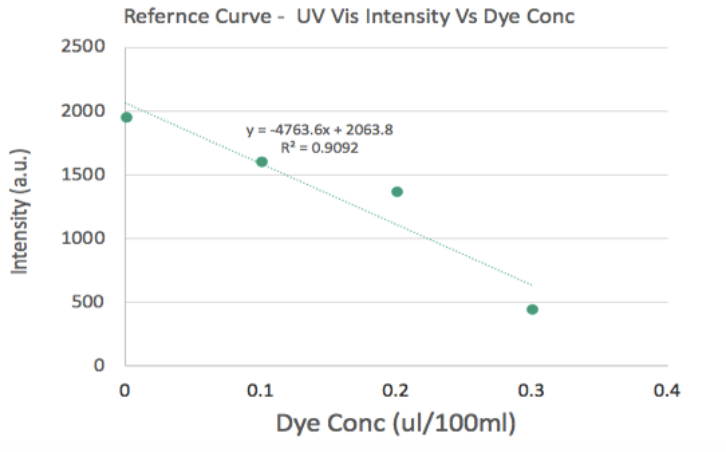

Figure 3-27: Intensity reference curve for MB concentration in distilled water

Then after coating the SS-Grid for 1 hour in 3 different concentrations (.1 micro liter, .2 micro liter, .3 micro liter) we measured the intensity after the release for 1 hour. Our results confirm that the higher initial concentration is, the less intensity after release will be as per chart 3-28 below:

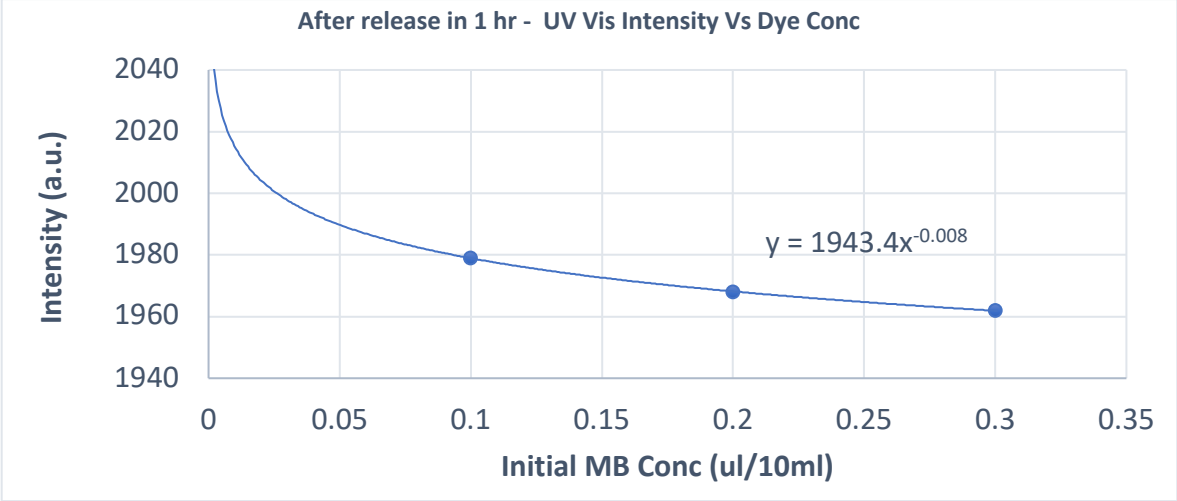

Figure 3-28: Decrease in concentration in the solution during coating phase in relation with time

3.5 Experiment of Release Curve on Fe80-SS20 without CNTs

We conducted this experiment to prove that the adsorption and release of the BM particles, happens by the CNTs only and not by any other factor. That's why for the above experiments of

SS-grid, and for Fe-SS, they all had CNTs grown on their surfaces. But for this specific experiment, the Fe80-SS20 has no CNTs on it. Therefore, we performed this experiment with the same sittings as per the previous trials, where the time was 5 minutes, 10 minutes and 15 minutes, and the concentration level of dye was 10 micro liters of 10 micro liter of BM.

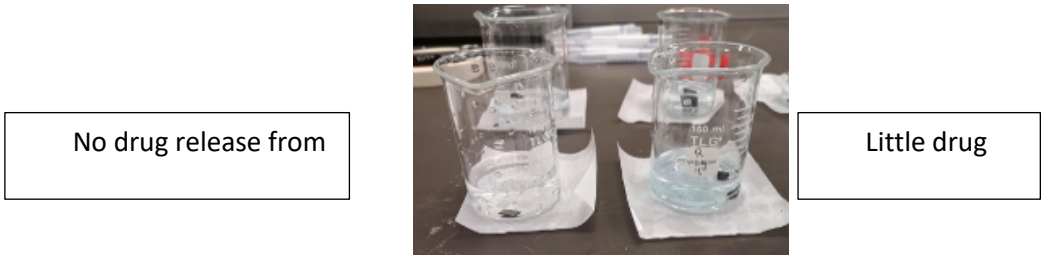

Figure 3-29: Comparison between Fe-SS with CNTs and without CNTs, we see on the right little drug release while on the left image there is no drug release.

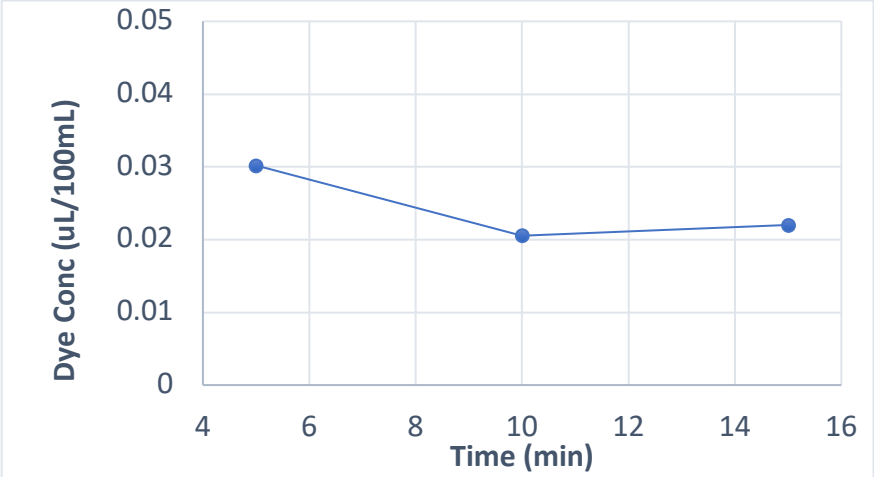

Figure 3-30: Intensity Measurements of Fe-SS without CNTs

Based on the table above we see that there is a very small change of the intensity during the release phase. This reflects that there was almost no adsorption of dye particles by this sample because there were no CNTs as we could clearly also see on the images below, where the 1st photo on the right shows almost a clear solution which has the Fe-SS without CNTs in it, but in comparison with the 2nd image we see some light blue color, which has the Fe-SS with CNTs. Also, the release curve below shows there is no change in the release based on different times. We did another analysis of the adsorption percentage between the following samples, SS-Grid, Fe80-SS20 with CNTs, Fe80-SS20 without CNTs. We found out that the adsorption percentage between the SS-grid and the Fe-SS with CNTs are similar, while on the other hand the Fe-SS

without CNTs is totally different from the other samples. This simply means, because of the CNTs which is common between the SS-grid and the Fe-SS with CNTs we have a similar range of adsorption percentage as per the Table 3-6 below:

SS	Fe & SS with CNTs	Fe & SS without CNTs
13.63%	17.95%	6.80%
16.54%	18.15%	4.60%
20.42%	24.75%	4.90%

Table 3-6: Comparison of coating capacity for SS, Fe-SS with CNTs and without CNTs

Also, this comparison confirms that we were successful in producing CNTs for the Fe80-SS20 sample.

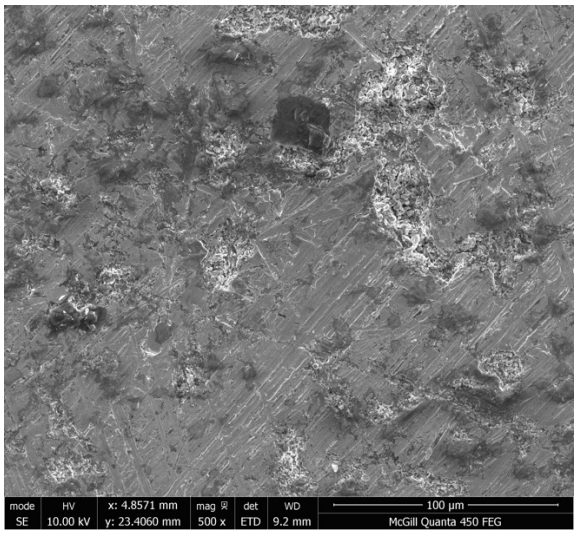

Figure 3-31: SEM image of bare Fe-SS without CNTs

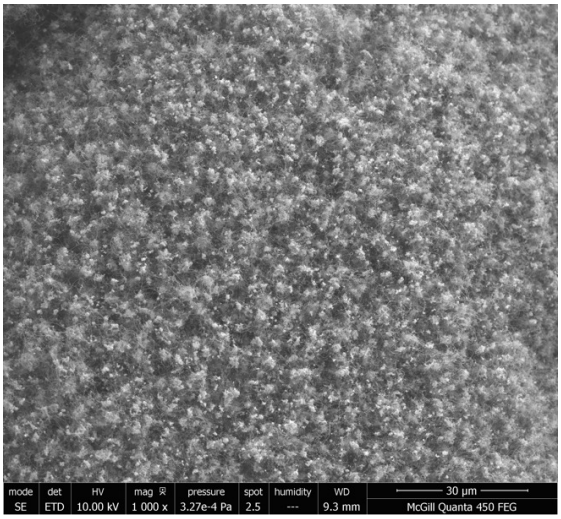

Figure 3-32: SEM image of Fe-SS with CNTs

For Figures (3-31,3-32) above, we see a direct comparison between Fe-SS without CNTs and with Fe-SS with CNTs before coating. We could clearly see the multi forest carbon nanotubes on the Fe-SS with CNTs on the 2nd image. For the 1st image we see a bare surface of the metallic structure without the presence of CNTs.

3.6 Experiment of (SS-Grid) Release Curve

We performed another experiment of the SS-grid, using the same reference curve above to compare our results and to ensure that we have a positive release curve. The immersion time here was different and shorter using 5 minutes, 10 minutes and 15 minutes, while the concentration of the dye was fixed at 10 micro liter as per Tables (3-7,3-8) below:

Samples SS	Coating Time	Concentration 10 micro liter / 20 ml water	Intensity before	intensity after release
1	0 min		2,061	
2	5 min			1780
3	10 min			1720
4	15 min			1640

Table 3-7: Table of Intensity after release for SS-Grid

Based on the table above, we notice that intensity of light decreases with time, which means the amount of dye particles released in the solution increases with time as well. Using the

equation from the previous reference curve **y=-4763.x+2063.8,** where y represents intensity and x represents concentration**,** then we calculated the concentration volume as per the table below:

x (time)	y (conc micro L/20mL)
5	0.059
10	0.072
15	0.089

Table 3-8: Table of Concentration Volume for SS-Grid during release phase

Then, we were able to conclude the release curve which confirms that more dye particles were released with time as per Figure 3-33 below:

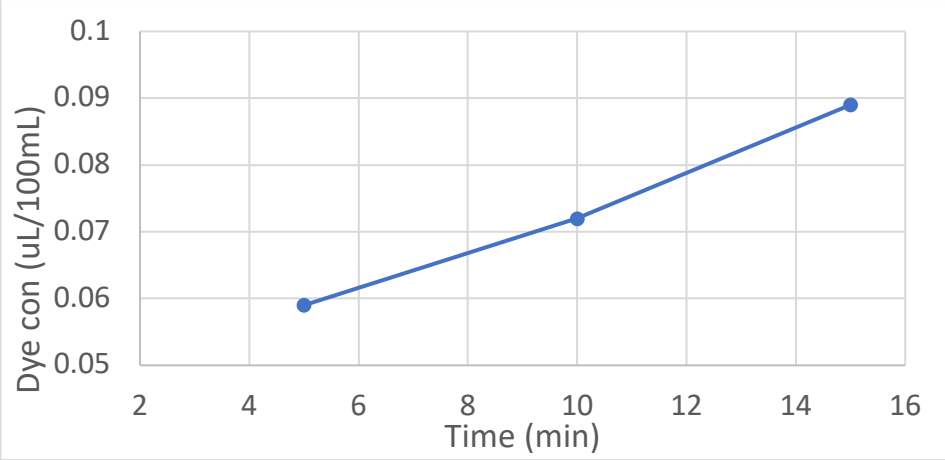

Figure 3-33: Positive Release Curve of SS sample

As per the analysis above, we clearly see that the intensity is decreasing with time during the release phase, which means in other words that the SS-grid CNTs are releasing more dye particles into the liquid which gives us gives us the curve with a positive slope as shown in the figure above.

3.7 Experiment of Release Curve of (Fe80-SS20) with CNTs

The settings were similar to the previous experience of the stainless steel (SS-Grid), where the times were 5 minutes, 10 minutes and 15 minutes with the same concertation level of 10

micro liter of BM as per Table 8-25. Also, we measured the intensity of the light with the use of UV-Vis and we noticed that the intensity decreased with time, which confirms that more dye particles are released from the Fe-SS sample the longer we wait as per the Table 3-9 below:

Samples Fe & SS with CNT	Coating Time (min)	Concentration 10 micro liter / 20ml water	Intensity before	intensity after release
Sample 1	0		2061	
Sample 2	5	10 ul		1691
Sample 3	10	10 ul		1687
Sample 4	15	10 ul		1551

Table 3-9: Table of Intensity after release for Fe-SS sample

Once again, we used the same equation from the previous reference curve **y=-4763.x+2063.8,** where y represents intensity and x represents concentration**,** then we calculated the concentration volume for the Fe-SS as per Table 3-10 below:

x (time)	y (conc micro L/100mL)
5	0.107
10	0.079
15	0.078

Table 3-10: Table of Concentration Volume for Fe-SS sample during release phase

By plotting the calculated concentration in relation with time, the result is a positive release curve for the Fe-SS sample as per Figure 3-34 below:

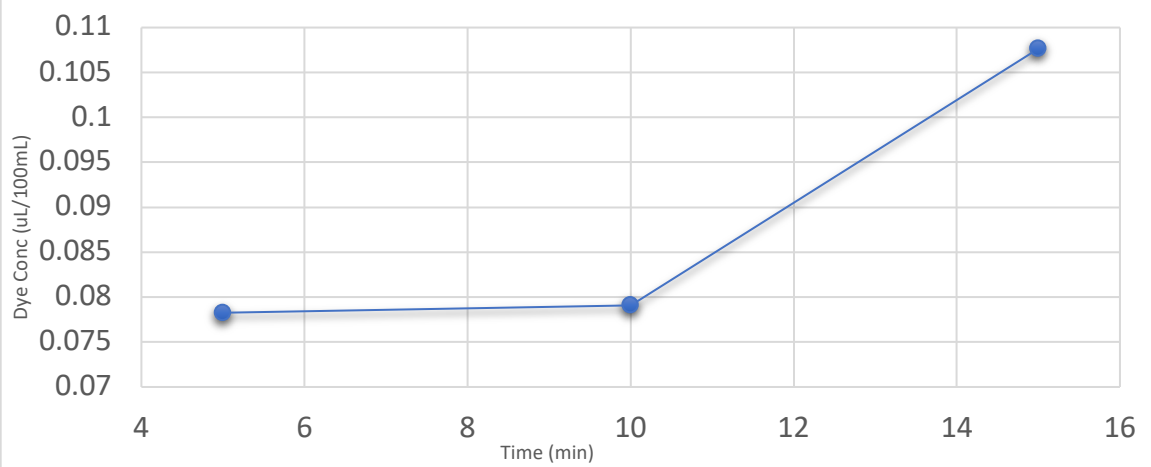

Figure 3-34: Positive Release Curve of Fe-SS sample

As per the analysis above, we clearly see that the intensity is decreasing with time during the release phase, which means in other words that the iron & stainless steel (Fe-SS) CNTs are releasing more dye particles into the liquid which gives us a curve of concentration of MB with a positive slope as per the figure above.

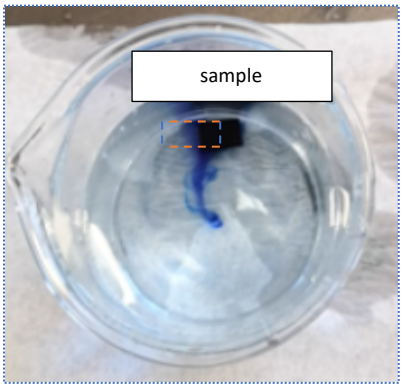

Figure 3-35: Image of Fe-SS substrate during Release Phase in distilled water

In addition to the mathematical analysis, we could also observe visually as per the image above, some MB dye are being released from the CNTs on the surface of Fe80-SS20 substrate in the distilled water.

3.8 Experiment: Establishing the 2nd Reference for Release Curve

For all the previous experiments and trials, we always used a distilled water. However, for the 2nd reference, we used 37% glycerin mixed with water to simulate the viscosity of the blood. We used a constant volume of glycerin/water of 100 ml, with different concentration percentage from .5 to 20 micro liter as per the Table 3-11 below:

Reference Curve Glycerine	Glycerine ml	Dye mico liter	1st measurement	2nd measurement	3rd measurement	Average
sample 1	100	0.5	2040	2038	2015	2031
sample 2	100	2.5	1982	1846	1722	1850
sample 3	100	5	1882	1727	1815	1808
sample 4	100	10	1787	1518	1615	1640
sample 5	100	15	1693	1460	1560	1571
sample 6	100	20	1529	1305	1346	1393.33333

Table 3-11: Experiment to conclude 2nd reference

We the average of three different measurements, then concluded the reference curve as per Chart 3-36 below:

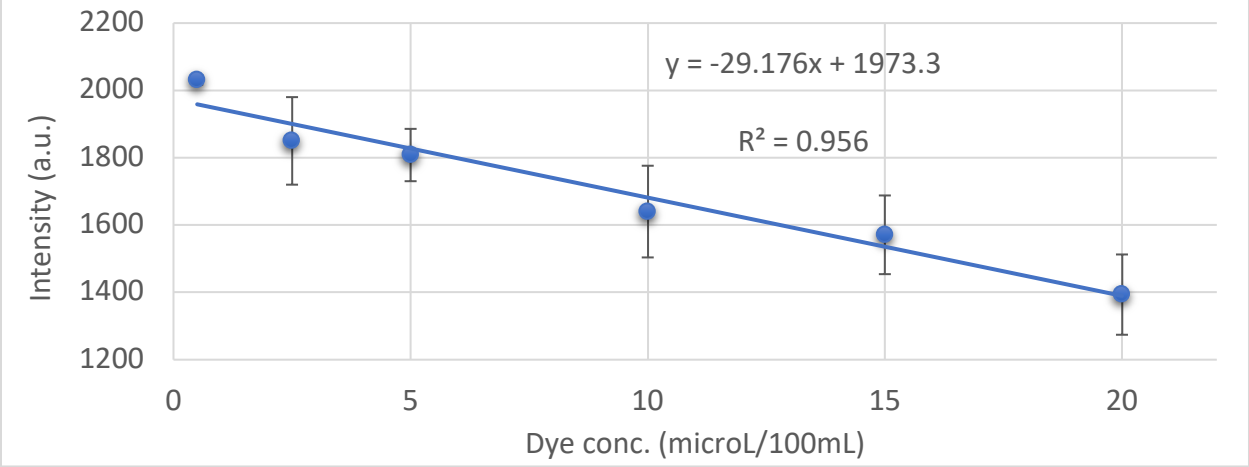

Figure 3-36: 2nd reference curve

3.9 Release Phase of Static Experiment on Fe80-SS20 with CNTs

For the coating time, we did different times such as 5 minutes, 10 minutes, 15 minutes and 20 minutes, then we did the release test in glycerin mixed with distilled water to establish the release curve by measuring the intensity after release using UV-Vis as per Figure 3-37 below:

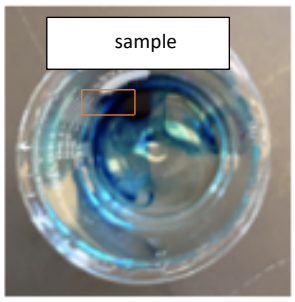

Figure 3-37: Image of Fe-SS sample during Release Phase in glycerin and distilled water

Samples Fe & SS	Coating Time in pure dye	Concentration 20 micro liter / dye	intensity after release
		1993	
Time 1	5		1664
Time 2	10		1551
Time 3	15		1236
Time 4	20		1230

Table 3-12: Table of Intensity after release in glycerin mixed with distilled water for Fe-SS sample

Then by using the equation from the 2nd reference we established, **y=29.176x+1973.3**, where y represents the intensity and x represents the concentration, we calculated the concentration volume for the Fe-SS as per Table 3-13 below:

Stat Release vs time _calc	
x (time)	y (conc micro L/100mL)
5	10.6
10	14.5
15	25.27
20	25.48

Table 3-13: Table of Concentration Volume for Fe-SS sample during release phase in glycerin mixed with distilled water

By plotting the calculated concentration in relation with time, the result is a positive release curve for the Fe-SS sample as per the Figure 3-38 below:

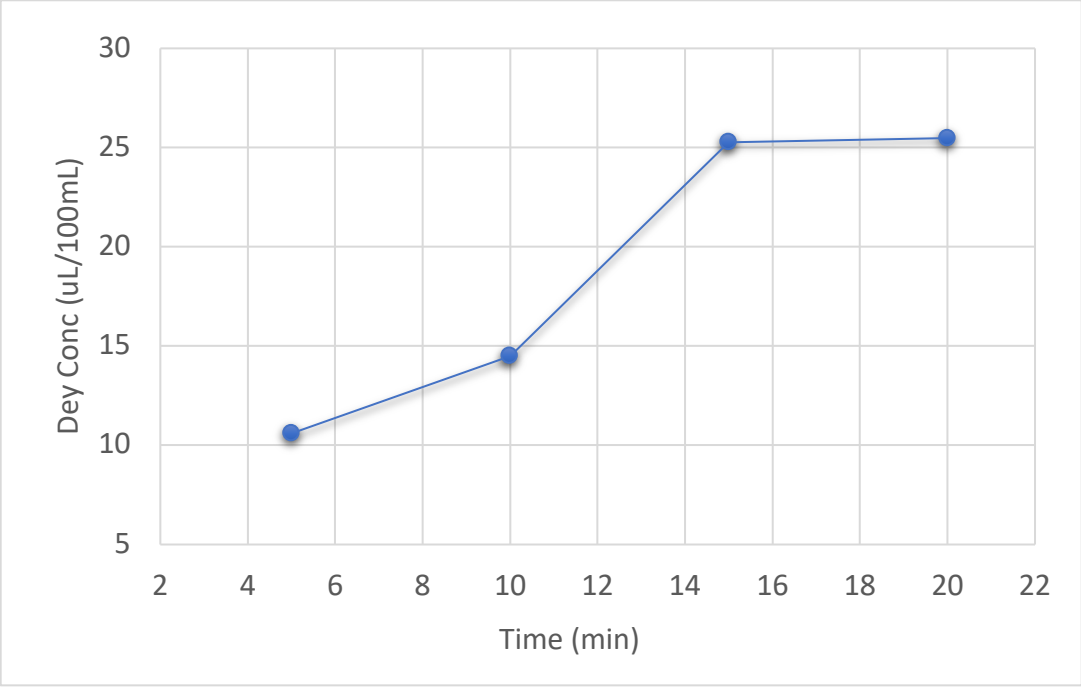

Figure 3-38: Positive Release Curve of Fe-SS sample

As per the analysis above, we clearly see that the intensity is decreasing with time during the release phase in glycerin mixed with distilled water to simulate the viscosity of blood, which means in other words that the iron & stainless steel (Fe-SS) CNTs are releasing more dye particles into the liquid which gives us the positive curve above.

3.10 Experiment of Motion on Fe80-SS20 with CNTs

For this experiment, we created a flow circuit and connected it to pulse generator to simulate the drug release inside the human body with approximate flowrate at 1450. The coating time was the same as the static trial of 5 minutes, 10 minutes, 15 minutes and 20 minutes, with concentration level of 20 micro liter.

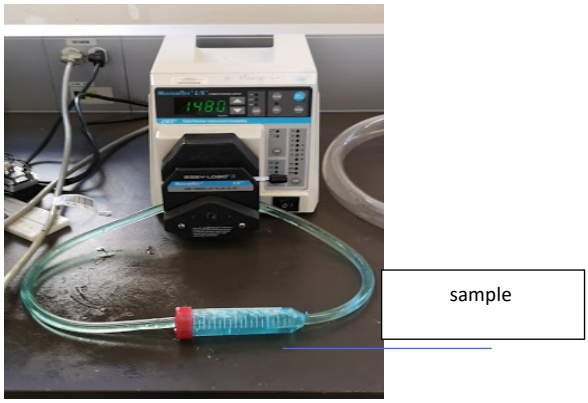

Figure 3-39: Release experiment of Motion for Fe-SS (Dynamic state)

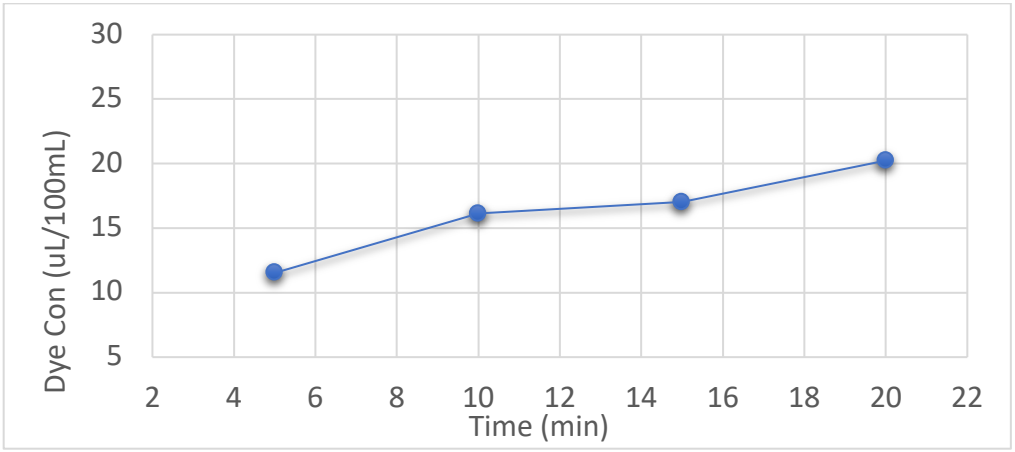

Figure 3-40: Intensity & Concentration levels for 1st Motion experiment on Fe-SS

Once again, we see a decrease of the intensity after release as the time increases. This confirms that the CNTs on Fe-SS were releasing continuously the BM particles in the solution

once immersed. We repeated this experiment twice more to confirm the positive release curve as per Figures 3-41 and 3-42 below.

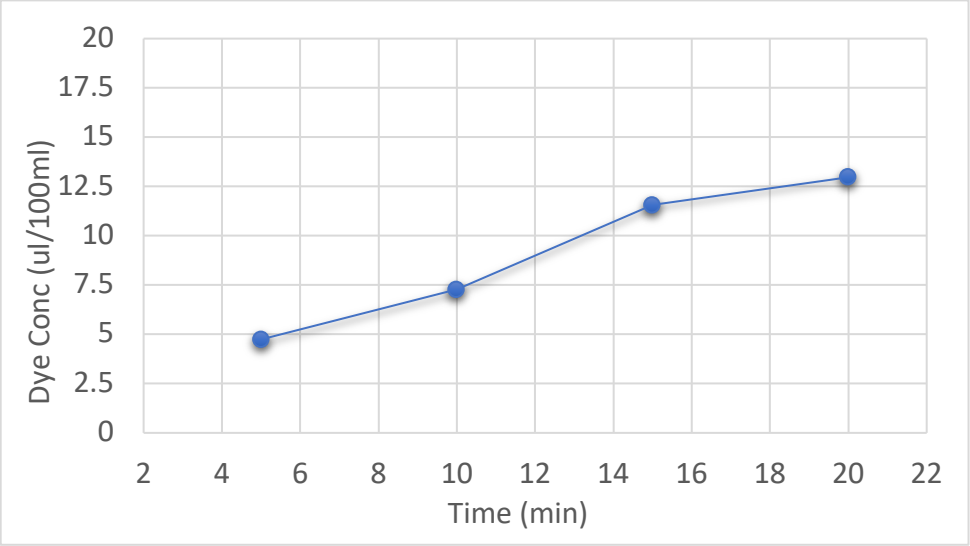

Figure 3-41: 2nd motion experiment & release curve for Fe-SS

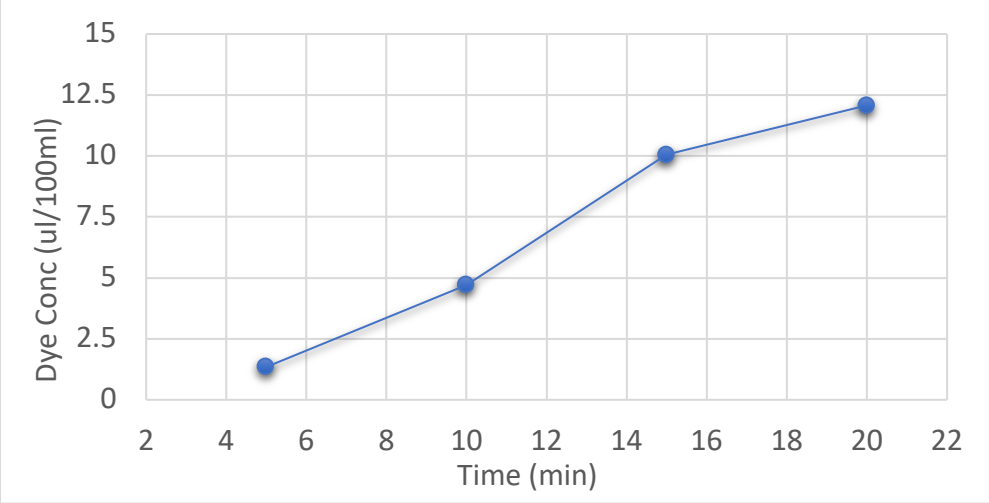

Figure 3-42: 3rd motion experiment and release curve for Fe-SS

As per the images above, we see a positive release curve as the intensity decreases with time, which means more dye particles are being released into the solution with time.

3.11 Tests

In order to validate the results from the previous experiments, we did a mathematical analysis to compare between measured concentrations and calculated concentrations. But before, we get

to the diffusion analysis, we define diffusion first. So, "**diffusion coefficient** (D) reflects how easily a substance can go into another substance a **unit** area in 1 s under the influence of a gradient of one **unit** $cm^2\ s^{-1}$". [33]

3.12 Diffusion Analysis for Static Experiment

The diffusion coefficient is very important for our validation because it describes how fast the dye particles can diffuse through the solution. Therefore, we used the following equation to calculate the concentrations in static phase

$$C=1/\frac{1}{\sqrt{4\pi Dt}} * e^{-x^2/4Dt} \quad [33]$$

C is concentration. t is time, x is distance , π is 3.14 [33]

D is the diffusion-coefficient of methylene blue in solution ($D_M = 1.663x10^{-10}m^2/s$) [33]

After using the equation above and the mentioned d-coefficient for MB, we had the following calculation for several concentrations volume at 5, 10, 15, 20 minutes:

Static									
Time	5 minutes		Time	10 minutes		Time	15 minutes	Time	20 minutes
4∏Dt	6.26618E+13		4∏Dt	1.25324E+14		4∏Dt	1.87986E+14	4∏Dt	2.5065E+14
Sqr	7915923.193		Sqr	11194805.94		Sqr	13710781.16	Sqr	15831846.4
1/sqrt	1.26328E-07		1/sqrt	8.93271E-08		1/sqrt	7.29353E-08	1/sqrt	6.3164E-08
x	0.01		x	0.01		x	0.01	x	0.01
x^2	0.0001		x^2	0.0001		x^2	0.0001	x^2	0.0001
4DT	1.9956E-07		4DT	3.9912E-07		4DT	5.9868E-07	4DT	7.9824E-07
C	10.98330945		C	13.16817838		C	21.85807977	C	24.1805995

Table 3-14: Calculations of concentrations volume during release phase in static experiment

And by plotting these figures in relation with time, we conclude a positive release curve similar to the experimental results as per Figure 3-43 below:

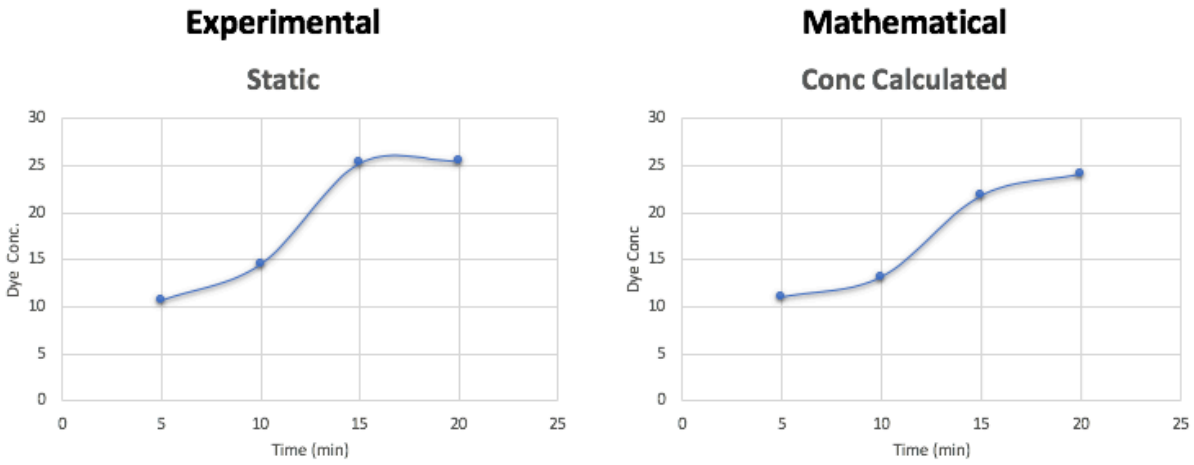

Figure 3-43: Release Curves (on left for practical experiment, on right for calculated results)

Based on the calculation of diffusion-coefficient, we found out the maximum error percentage between the practical and calculated results is approximately 13.6%, which is an acceptable figure to validate the results from the previous experiments.

Chapter 4

4.1 Conclusion

We successfully met all the primary and secondary objectives in this study, where CNTs were successfully grown on SS-grid and Fe-SS substrates using CVD technique with modifications for Fe-SS substrate such as etching with acid for 10-15 minutes and pre-heat treatment for 30 minutes at 800 degree. Also, coating on CNTs was done and was investigated qualitatively and quantitatively, where MB loading was higher compared to bare substrate. Additionally, release of MB was done in water and in water/glycerol media with various time intervals and shown a proportionality between time and release. Finally, release was done under static and dynamic flow conditions and found that forced release gave up more MB. We successfully established strong proof of concept for all key objectives. we could achieve a CNT-forest structure that is strongly adherent to bio-degradable stent supports, which supports the possibility of controlled absorption-desorption of a drug. The controlled desorption proved to be possible in both water and glycerin mix simulating blood viscosity. This represents a good step to the target in creating a biodegradable and drug eluting stent made of Fe80-SS20, as an ideal alternative to the bare metal stents and polymer based biodegradable stents.

4.2 Suggestions for Future Studies

Future work of this project is to optimize the protocols for the growth of carbon nanotubes, where we could control the structure of the CNTs, the type of the CNTs and the size of the CNTs which will be an important factor in the drug coating and drug release in the next phase. For the drug coating and release, good results were obtained. However, the next step will be to work on more sophisticated coating methods such as plasma-treated coating and ultrasonic spray coating, which will give us more control of the amount of the drug coated to the CNTs and more control of the drug release. Once the optimization of the fabrication methods is achieved, we would be able to start the in vivo tests which will bring us a lot closer to the finalization of the general project which is the drug-eluting biodegradable stent made of a combination of iron and stainless steel.

4.3 Limitations and Challenges

More sophisticated coating equipment is needed for this project, also more Fe-SS samples are necessary to conduct more CNTs growth experiments and coating trials. Scanning electron microscopy (SEM) analysis is still costly and can't be done for every Fe-SS sample after each CNTs production experiment. Transmission electron microscopy is also important for more in depth material analysis, but it was not available at that time as it requires special and long training, cost is high as well. There was also an interruption of CNTs production as some upgrade was needed for the furnace, this did not allow more production of CNTs on Fe-SS samples.

APPENDIX A: Summary of the Biodegradable Metallic Stent Based on Micro galvanic Effect

Since 1986, there has been a trend to switch from the permanent stents to the biodegradable stents. This is why a large research effort was made on polymer-based materials as key replacements to the metallic design of the new biodegradable stent. However, polymer did not generate much success and most of the projects were abandoned as was the case of the last research at Abbott. Some of the key reasons behind the failure of the polymer-based stent is the fact that polymers have lower mechanical properties in comparison with metals. This leads to large strut thickness, which causes limitation in elastic recoil and not enough radial strength. Not to forget that, the whole point behind replacing metallic stent by biodegradable polymer-based stent was to avoid the complications such as thrombosis or late in-stent restenosis. However, because of the thick strut of the polymer-based stent, it will still cause these complications which we were trying to avoid in the first place. In other words, polymer based stents have the same complications as the metallic stents, and even worse, because the late effects of the polymer degradation on vascular tissue are still not known[34]. Therefore, other alternatives such as the use of two metals together (iron & stainless steel) to benefit from their oxidative properties for degradation have been initiated (Frattolin 2019). However, current challenges include the large and thick strut of these two metals and the development of a compatible coating to operate in conjunction with the stent. Frattolin et al in 2019 used the cold gas dynamic spraying method (CGDS) to create a stent with fine grain material [34].

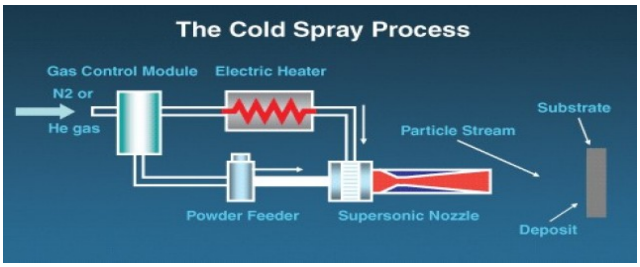

Figure A-1: : Cold Spray System, preheated high-pressure gas propels micron-sized particles of powder at high speed 300–1500 m/s. Then powder is exposed to the target to form a coating over the substrate, which creates microstructure with grain sizes in the micron to submicron range that have high strength and excellent wear properties [34]

The main reason behind choosing a mixture of iron and stainless steel for the new biodegradable stent, is because the iron, which is anodic, when combined with the cathodic

stainless steel 316L, produce a galvanic couple when exposed to blood electrolyte and start corroding each other at possibly controlled rate and controlled duration. The degradability rate of the novel stent by is controlled with the percentage of iron vs. stainless steel 316L. The proposed coating constitutes a new drug delivery paradigm compatible with this substrate.

A.1 Materials and Methods

More specifically stainless steel 316L powder with a particle size of 43.7+-17μm, and 99% pure iron powder with a particle size of 25.2+-14.6μm are combined as per Figure A-2 below:

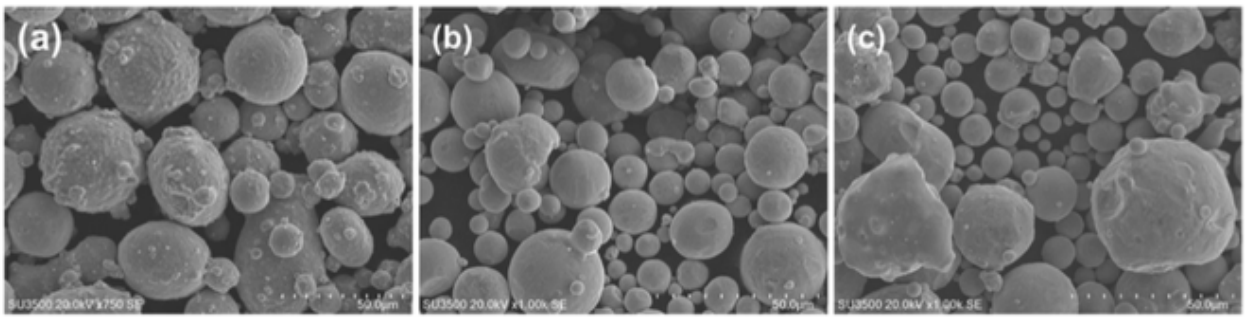

Figure A-2: Scanning Electron Microscopy Analysis [34], a) iron particles, b) SS particles, c) iron and SS particles. As can be seen on the left picture, it is the particles of stainless steel, while the middle picture shows the particles of the iron, and finally the last picture shows the combination of 80% iron particles with 20% stainless particles.

A.2 Testing

Several testing such as chemical composition and microstructure trials were conducted on the new material. We summarize below the tests that have a relation with the proposed new coating. Electron backscatter diffraction (EBSD) and (SEM) scanning electron microscopy were used to analyze the porosity and size of grains on different substrates including 20Fe-80SS [34]. We chose 20Fe-80SS because of its optimal corrosion property.

a) Microstructure Testing

Scanning electron microscopy (SEM) was used to analyze the surface of the sample 20Fe-80SS as per Figure A-3:

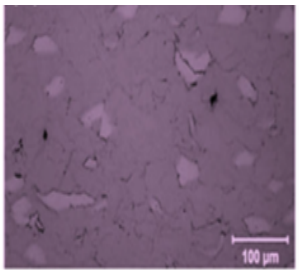

Figure A-3: Heat Treatment Processing. Image represents the non-heat-treated sample 80Fe-20SS was analyzed, where the dark and light areas of the images represent the Fe& SS particles[34]

The samples produced with 20Fe-80SS showed little porosity with average of .30+-.11 and .31+-.24% [34]. This porosity is minimal and as shown subsequently allows for the formation of dense carbon nanotubes forests (for drug carrying capacity).

b) Static Corrosion Test

Degradation tests were performed using samples into a salt solution (HBSS), which simulates the blood plasma to test the corrosion rate after 7-9 days, 20Fe-80SS and 100Fe.Visually, it was clear that there was a major oxidation for all samples as per Figure A-4 below:

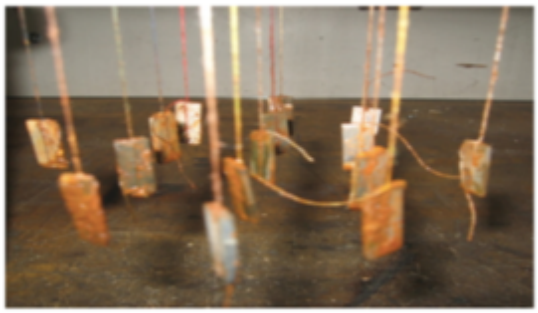

Figure A-4: Corrosion Test, samples of 20Fe-80SS after immersion in salt solution for 7-9 days [34]

It was found out that the 80Fe-20SS had the greatest mass loss with an average corrosion rate of .17 mm, as per Figure A-5:

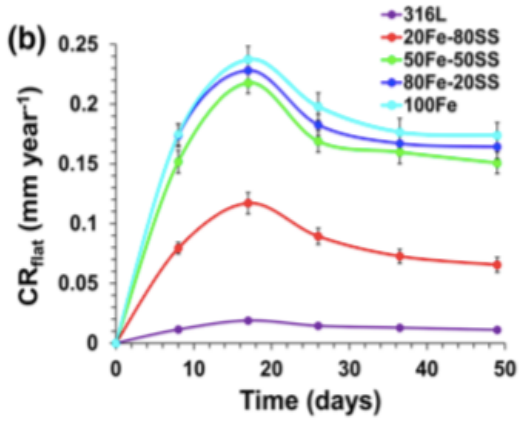

Figure A-5: Corrosion Rate Evaluation [34]

c) Galvanic Corrosion Test

To evaluate the effectiveness of the galvanic effect, the team performed galvanic corrosion experiments. The 80Fe-20SS had the best galvanic effect with a corrosion rate of .48 mm as compared to other ratios as per Figure A-6 below [34]:

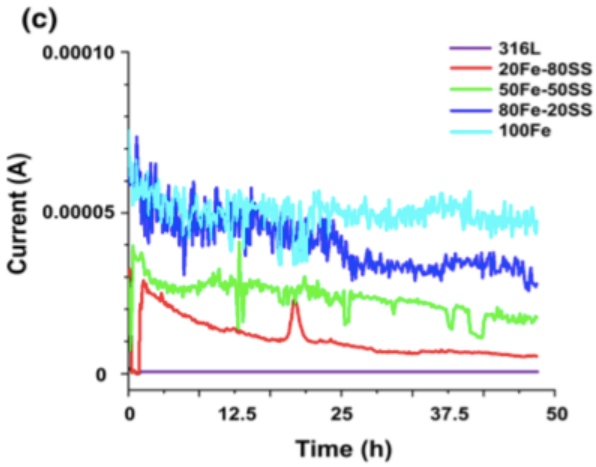

Figure A-6: Galvanic Rate [34]

The new coating should then remain stable for a period of time corresponding to these time scales. In other words, in practice, since a treatment varying between one and two years is targeted, the carbon nanotubes coating should keep their structure during that

time frame.

APPENDIX B: Summary of Thermal CVD method of carbon nanotube synthesis on stainless steel 304

Carbon nanotubes have wide range of applications such as in electrical, sensor, water treatment and medical applications[25]. That's why for these applications, we need a conducting substrate such as stainless steel (SS) for the growth of carbon nanotubes[25], since stainless steel has high content of iron. There are various way of CNTs synthesis methods including plasma-enhanced chemical vapor deposition , thermal chemical vapor deposition (CVD), and partial oxidation of methane…[25]. For most of cases, the SS sample must be treated before CNTs growth, the typical treatments include etching in acids and pre heat treatment. In this study, Professor Meunier's team used chemical vapor deposition without the need of an extra catalyst to grow CNTs. They simplified the process by growing multi-walled nanotubes (MWNTs) directly on the surface of SS 304 by using CVD [25]. For the chemical vapor deposition furnace, they used Lindberg/Blue HTF 55000 as per the image below:

Figure B-1: CVD furnace from Lindberg/Blue, used for the production of CNTs at high temperature [25]

B.1: Experiments and Methods

The following protocol for the synthesis of CNTs directly on the surface of SS 304 without any additional catalyst.

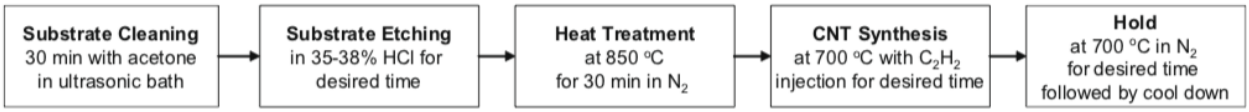

Figure B-2: CNTs Growth Protocol on SS 304 [25]

The process starts with cleaning the SS sample with acetone and then sonicate for 30 minutes. Then, the SS sample is etched with acids containing 35-38% HCL for various times. After etching, the SS sample is pre heat treated for 30 minutes inside the furnace at 850 degree. Then, the growth protocol begins with placing the sample inside the furnace and expose it for high temperature at 700 degree, then injecting acetylene for usually 5 minutes, then the last step purging the acetylene with nitrogen for desired time (usually for 15 minutes) before the cool down step.

B.2: 1st experiment

In the study of (Baddour, C.E., et al), they conducted several experiments based on different growth temperatures (650-degree, 700 degree and 800 degree), then they used scanning electron microscopy for the characterization of the surfaces of SS substrates. All SS samples were etched for 5 minutes with HCI and pre-heat treated at 850 degree for 30 minutes. They had good results at 700- and 800-degrees temperature as per the SEM images in Figure B-3 below:

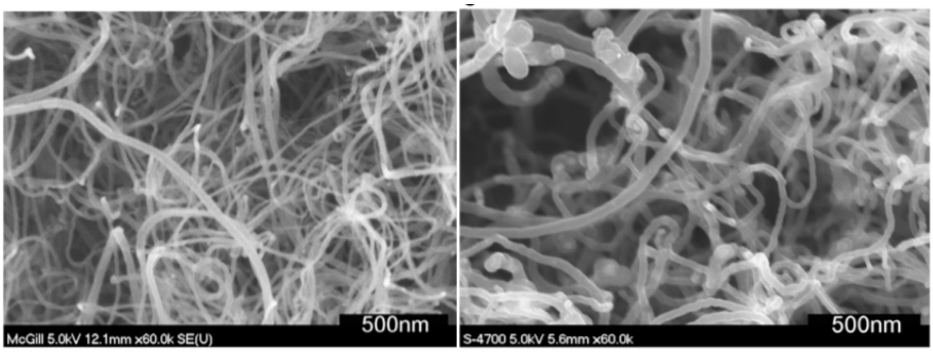

Figure B-3: SEM images (left image CNTs growth at 700-degree, right image CNTs growth at 800 degree) [25]

B.3: 2nd experiment

Another experiment was conducted to test the effect of different HCI etching time on the growth of CNTs on SS samples, while they kept the growth temperature at 700 degree and pre heat treatment at 850 degrees for 30 minutes, as per Table B-1 below:

HCI etching time (min)	1	3	5	10
% CNT coverage	7	38	92	97

Table B-1: Effect of HCI etching time on CNT coverage [25]

As per the results above, they had the most CNTs growth when they did the etching time at 10 minutes.

B.4: 3rd experiment

In this experiment, the growth temperature was kept at 700 degree but with two different growth time (10 minutes and 20 minutes). The etching time was 5 minutes and the pre heat treatment was 850 degree for 30 minutes. They concluded that they did not notice any increase of MWNTs with the 20 minutes growth time in comparison with the 10 minutes growth time as per the SEM images in Figure 2-4 below:

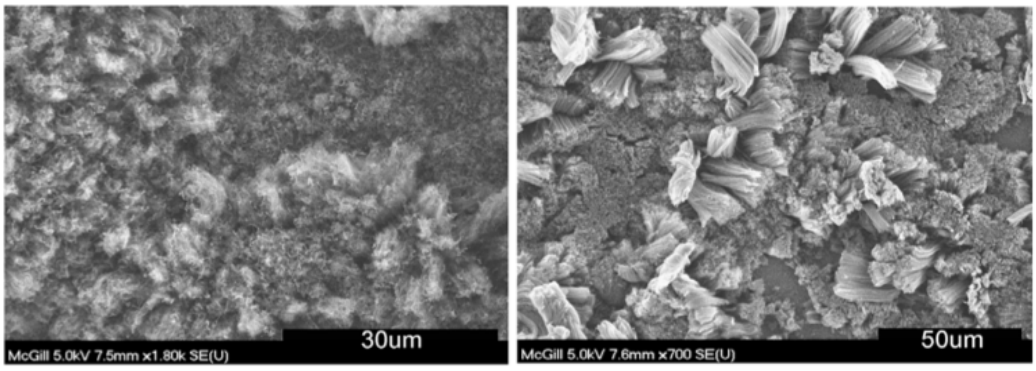

Figure B-4: SEM images (Left image @ growth time of 10 minutes, right image @ growth time of 20 minutes) at 700 degree temperature [25]

B.5 Conclusion

As per the previous experiments, it was found out the least amount of amorphous carbon at growth temperature of 700 degree for a pre heat treated sample via comparison with another sample that was not pre heat treated [25]. All the CNTs produced were multiwalled with (20 to 70 nm diameters). The output from the pre heat treatment was to produce nanometer scale grain structures to create a suitable growth site instead of using a separate catalyst [25]. The team also etched the SS samples in HCI at different times (1,3,5,10) minutes to examine any change on the growth of CNTs. They demonstrated that the longer the etching time was, the more CNTs were produced. They also performed another experiment with different acetylene injection times of (1.5,3,5) minutes, where they concluded that the best CNTs growth and density was with 5 minutes of acetylene injection. The 10 minutes injection time did not make any changes either. They also conducted different CNT growth times (0,10,20,30) minutes after the injection of acetylene, they found out that larger and longer bundles of CNTs were observed as the growth increased reaching length up to 30-40 micro meter at growth time of 20 minutes [25]. It was concluded that the CNTs were denser as the growth time increased with diameters of 5-30 nm as per the SEM image in Figure B-5 below:

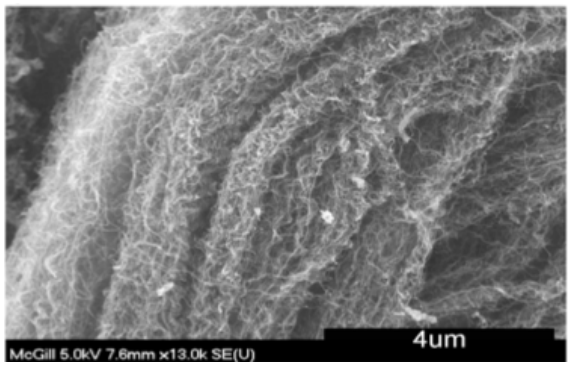

Figure B-5: SEM image of CNTs bundle at growth time of 20 minutes [25]

Finally, it was observed that at 30 minutes growth time, they had a uniform layer of CNTs on the SS surface as per the SEM image in Figure B-6 below:

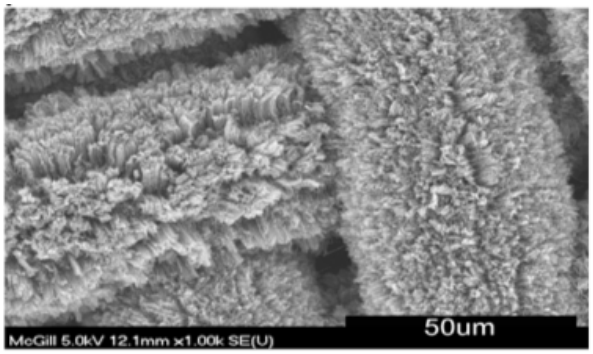

Figure B-6: SEM image of uniform CNTs bundle on SS substrate [25]

Appendix C: Summary of methodology for oxidative heat treatment of 316L stainless steel for effective catalytic growth of carbon nanotubes

As the need for the massive production of CNTs is growing especially for commercial purposes, it is important to find a way to integrate it into the existing manufacturing protocols while keeping the cost to minimum [35]. Stainless Steel contains other metals such as iron, nickel…etc. Additionally, SS is covered with protective film layer made of chromium oxide [35], where chromium does not react well with hydrocarbon gases such as acetylene which is the main source of CNTs production. Therefore, pretreatment procedures such as acid etching, heat treatment, plasma treatment and laser treatment are necessary to breach the external protection layer on the surface of SS [35], before the growth of CNTs [35]. As per the study, it has been proven that iron and nickel layers underneath the chromium oxide layer, become suitable catalyst for the growth of CNTs due the increase of the size of grain particles. The pre-treatment is important as well to break the formed large particles and to transform it into thinner catalyst seeds for the facilitation of CNTs [35]. In the study of C Zhuo from Northeastern University in Boston, they performed surface morphology tests, surface elemental analysis and electrochemistry tests to prove the benefits of the pre-treatment procedures for the production of CNTs, and to establish the relation between the pre-treatment phase with the reactivity changes of the surface of SS for the synthesis of CNTs [35].

C.1 Stainless Steel heat treatment

For this experiment, a 316L SS mesh was used as per Figure C-1 below:

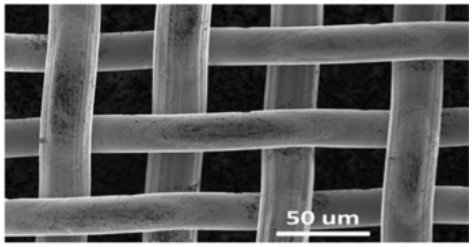

Figure C-1: SEM Image of SS Mesh [35]

The SS mesh contained 16–18.5% Cr, 10–14% Ni, 2–3% Mo, <2% Mn, <1% Si, <0.045% P, <0.03% S, <0.03% C [35] in addition to Fe. The samples were prepared into different sizes such as 1cm*3cm, 10cm*30cm. Then, all samples were sonicated for 10 minutes for cleaning purposes. Then, they were dried before exposed to a temperature of 800 degree. The only oxidation gas they used was oxygen for 1, 5, 10 and 20 minutes separately [35].

C.2 Characterization of CNTs

They used scanning electron microscopy (SEM) to analyses the surface morphology and elemental composition of the sample as per Figure C-2 below:

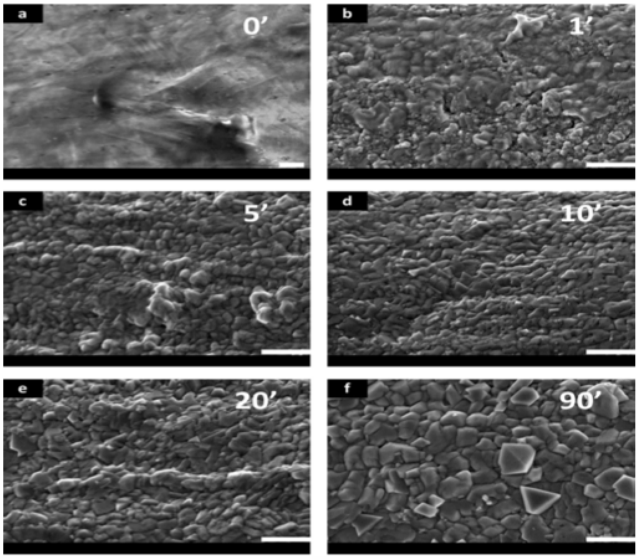

Figure C-2: a) Image 0 min, b) Image 1 min, c) Image 5 min, d) Image 10 min, e) Image 20 min, f) Image 90 min [35]

The images above show 2 types of surface morphology [35], the 1st one was with individual surface extrusions and the 2nd one with other bumps of larger coverage. The structures were in the shape of dome without clear borders especially for all pre-treatments less than 20 minutes. But for the pre-heat treatment of 90 minutes, there were more sharp edges and the sizes were approximately 200 nm [35].

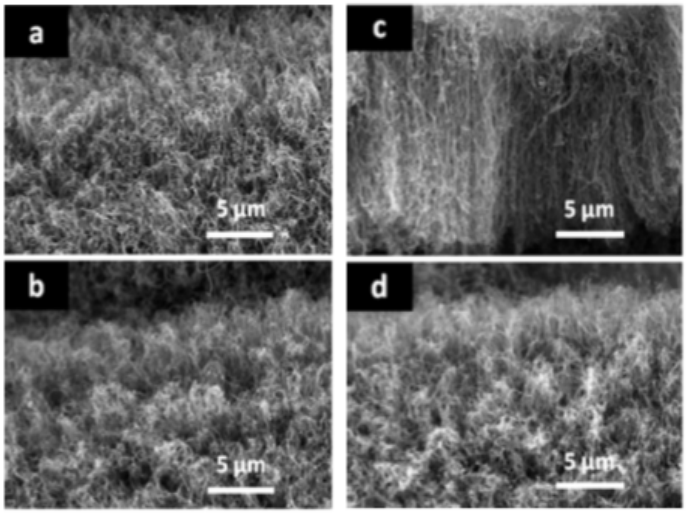

Figure C-3: Effects of the heat treatments on the reactivity of substrate surfaces, a) 1 min, b) 5 min, c) 10 min, d) 20 min [35]

The thicker the multi forest carbon nanotubes were respectively [35]. However, after 20-30 minutes, the team observed the opposite as they were less CNTs grown for 90 min pre-heat treatment. The explanation was that, anything after 20-30 min, will thicken the passive layer and increase oxidation / Corrosion resistance, which leads to reduction of SS surface reactivity. Zhuo and his team conducted several experiments without oxidative pre-heat treatment, and they were not successful in fabricating CNTs on the 316LSS, until they removed the protective chromium oxide layer and exposed the metal underneath, where they had good growth of CNTs [35]. They also noticed that they could control the growth, thickness and length of the CNTs by varying the heat treatment time. For instance, the mean diameter of the CNT changed as the duration changed. The initial results were as per the following [35], for 1 min, 27 ± 8.5, for 5 min, 22 ± 8.5, for 10 min, 20 ± 9.3, for 20 min, 20 ± 7.6 nm. Also, they noticed that CNT diameter is affected by the particle size of the grain, and anything after 30 min, could lower the growth of CNTs due to the fact that there is less catalyst particles suitable for CNT growth [35]. Therefore, any longer oxidative heat treatment time results to higher degrees of metal oxidation which causes the blockage of the CNT synthesis [35]. In Figure 3-3, is shown that highest roughness of the surface of the SS substrate was reached at 20 minutes, which makes a perfect surface for the synthesis of CNTs. On the other hand, regarding the figure above, we see that the longest carbon nanotube was reached at 20 minutes as the diameter gets smaller [35]. Additionally, the Northeastern University team found out that changing the pre-heat treatment could affect the architecture of the CNTs. However, they noticed a consistency in growing vertical, perpendicular to the surface, and thick MFCNTs when the pre-heat treatment was 10 minutes, before the injection of carbon source gases to the reactor, as seen in the figure above [35]. The result was brush-like CNT arrays produced vertically to the SS surface with height of 20nm. This is appropriate for electronics applications and filtration applications where direct contact between the CNTs and substrates are required [35]. On the other hand, in this study, it is shown that when the samples were pre-treated for shorter time than 10 minutes, no vertical multi forest of CNTs were

produced. In conclusion, the team suggests that vertical growth of CNTs can be generated based on combined effects of optimized catalyst roughness, particle size and nanotube diameters.

Appendix D: Summary of Synthesized multi-walled carbon nanotubes as a potential adsorbent for the removal of methylene blue dye: kinetics, isotherms, and thermodynamics

In the study of Selen, V., et al from the Chemical Engineering Department at the University of Firat in Turkey, demonstrated the high capacity of CNTs to be used as absorbent of methylene blue. These results confirm the potential of the CNTs to be used in many applications such as water treatment, filtration and drug coating as well [36]. Many studies have proven that multi-walled carbon nanotubes are very effective adsorbent of methylene blue [36]. Multi walled carbon nanotubes (MWCNTs) were produced using chemical vapor deposition method, and the surface of the carbon nanotubes (CNTs) was analyzed using transmission electron microscopy (TEM). They also determined the factors to control the adsorption rate by MWCNTs such as pH, contact time, dosage, concentration and temperature [36]. CNTs have excellent physiochemical stability, high selectivity, large surface areas, small size, hollow and layered structures which provide high capacity for adsorption [36]. In this study Selen, V., et al , they evaluated the adsorption capacity of MWCNTs for removing MB from water.

D.1 Methods and Results

MWCNTs and 600 ml of the MB solution were placed in thermostatic water bath, then they the solution was mixed for 1 hour at 600 rpm [36]. After that, in order to measure the effect of contact time, several trials were performed with the following factors, different time ranges from 0 to 1 hour, 0.25 g/L of MWCNTs, MB concentration of 40mg/L, PH 5.5-11. For the determination of the effect of MB concentration, they performed the following, MWCNTs = 0.25 g/L, MB concentration were 20 and 60 mg/L. For the determination of the effect of the temperature of the MWCNTs, they performed the following, MWCNTs = 0.25 g/L, MB concentration = 40 mg/L, 1st temp at 293 k and 2nd temp at 323 k. Then, the team used UV-vis spectrometer to measure the amount absorbed of MB by the CNTs as per the figure D-1 below:

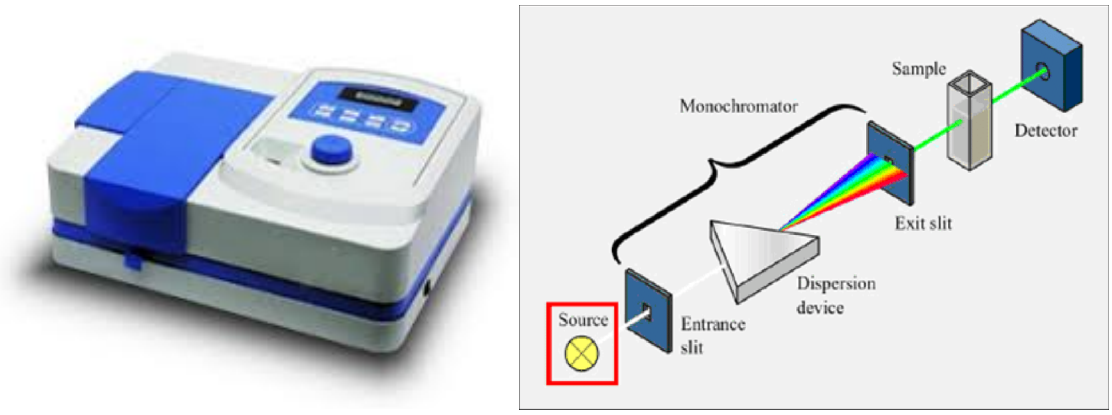

Figure D-1: UV-Vis: The absorption or reflectance in the visible range directly affects the perceived color of the chemicals involved. In this region of the electromagnetic spectrum, atoms and molecules undergo electronic transitions. [36]

By calculating the difference of the intensities before absorption and after, they were able to confirm that the MWCNTs were able to attract the MB particles and hold on it. They also noticed that the longer the dipping time is, the more adsorption resulted. The team concluded that MWCNTs have excellent potential to remove the MB particles from water. They also noticed that adsorption increased with time until it reached the maximum after 1 hour of dipping. This reflects the diffusional properties of the CNT. It is those diffusional properties that we propose to exploit to develop a coating for controlled chemical compound release of a medical drug.

References

1. Canfield, J. and H. Totary-Jain, *40 years of percutaneous coronary intervention: History and future directions.* Journal of Personalized Medicine, 2018. **8**(4).

2.google.com/search?client=safari&channel=mac_bm&biw=1345&bih=617&tbm=isch&sxsrf=ACYBGNSsVgyl4SVmAWNPPsdnUDEmJLlJ-w%3A1572373607540&sa=1&ei=Z4S4XcO6IIGt_Qa_uZH4Ag&q=image+of+magnesium+stent&oq=image+of+magnesium+stent&gs_l=img.3...8377.9165..9397...0.0..0.96.423.6.....0....1..gws-wiz-img.....35i39j0j0i30j0i24.Cl-QySlhSEQ&ved=0ahUKEwiDitOSjMLlAhWBVt8KHb9cBC8Q4dUDCAY&uact=5.

3. *https://www.mayoclinic.org/tests-procedures/coronary-angioplasty/about/pac-20384761*.

4. Hytönen, J.P., et al., *Biodegradable coronary scaffolds: Their future and clinical and technological challenges.* Cardiovascular Research, 2018. **114**(8): p. 1063-1072.

5. Mao L, Y.G., Wang S, Niu J, Wu G, Ding W. , *A novel biodegradable Mg-Nd-Zn-Zr alloy with uniform corrosion behavior in artificial plasma. Mater Lett 2012;88:1–4.*

6. Rukshin V, S.P., Cercek B, Finkelstein A, Tsang V, Kaul S. , *Comparative antithrom- botic effects of magnesium sulfate and the platelet glycoprotein IIb/IIIa inhibitors tirofiban and eptifibatide in a canine model of stent thrombosis. Circulation 2002;105:1970–1975.*

7. Singhvi, M.S., S.S. Zinjarde, and D.V. Gokhale, *Polylactic acid: synthesis and biomedical applications.* Journal of Applied Microbiology, 2019. **127**(6): p. 1612-1626.

8. Campos CM, M.T., Iqbal J, Zhang YJ, Onuma Y, Garcia-Garcia HM, Haude M, Lemos PA, Warnack B, Serruys PW., *Bioresorbable drug-eluting magnesium-alloy scaffold for treatment of coronary artery disease. IJMS 2013;14:24492–24500.*

9. Chaabane C, O.F., Virmani R, Bochaton-Piallat ML, *Biological responses in stented arteries. Cardiovasc Res 2013;99:353–363.*

10. Cassese S, B.R., Ndrepepa G, Kufner S, Wiebe J, Repp J, Schunkert H, Fusaro M, Kimura T, Kastrati A. Cassese S, Byrne RA, Ndrepepa G, Kufner S, Wiebe J, Repp J, Schunkert H, Fusaro M, Kimura T, Kastrati A. , *Everolimus-eluting bioresorbable vascular scaffolds versus everolimus-eluting metallic stents: a meta-analysis of randomised controlled trials. Lancet 2016;387:537–544.*

11. *https://www.kyoto-mp.co.jp/en/igaki_tamai_stent.html*.

12. Nishio S, K.K., Igaki K, Okada M, Kyo E, Tsuji T, Takeuchi E, Inuzuka Y, . Takeda S, Hata T, Takeuchi Y, Kawada Y, Harita T, Seki J, Akamatsu S, Hasegawa S, *Long-term (>10 Years) clinical outcomes of first-in-human biodegrad- . able poly-L-lactic acid coronary stents: Igaki-Tamai stents. Circulation 2012;125: . 2343–2352.*

13. *Five-year clinical and functional multislice computed to- . mography angiographic results after coronary implantation of the fully resorbable . polymeric everolimus-eluting scaffold in patients with de novo coron.*

14. *Late stent recoil of the bioabsorbable everolimus-eluting coronary st.*

15. Tenekecioglu E, F.V., Bourantas CV, Silva RC, Onuma Y, Yılmaz M, Serruys PW, *Bioresorbable scaffolds: a new paradigm in percutaneous coronary intervention. BMC . Cardiovasc Disord 2016;16:38.*
16. Heublein B, R.R., Kaese V, Niemeyer M, Hartung W, Haverich A. , *Biocorrosion . of magnesium alloys: a new principle in cardiovascular implant technology.*
17. Erbel R, D.M.C., Bartunek J, Bonnier J, Bruyne de B, Eberli FR, Erne P, Haude M, Heublein B, Horrigan M, Ilsley C, Bo¨se D, Koolen J, Lu¨scher TF, Weissman N, Waksman R. , *Temporary scaffolding of coronary arteries with bioabsorbable magnesium stents: a prospective, non-randomised multicentre trial.*
18. Haude M, E.R., Erne P, Verheye S, Degen H, Vermeersch P, Weissman N, Prati F, . Bruining N, Waksman R, Koolen J. , *Absorbable Metal Scaffold (DREAMS) in patients with de novo coronary lesions: 3- . year results of the prospective, multicentre, firstin-man BIOSOLVE-I trial. . EuroIntervention 2016;12:e160–e166.*
19. WuY, S., WangQ,GeL,XieJ,HuX,SunA,QianJ,GeJ., *Comparisonofacute recoil between bioabsorbable poly-L-lactic acid XINSORB stent and metallic stent in porcine model. J Biomed Biotechnol 2012;2012:1.*
20. ChenJH, W., ShenL,ZhangF,YaoZF,YinJS,JiM,WangQB,GeL,QianJY,Hu X, Xie J, Ge JB. , *First-in-man implantation of the XINSORB bioresorbable sirolimus- eluting scaffold in China. Chin Med J 2015;128:1275–1276.*
21. Ang, H.Y., et al., *Mechanical behavior of polymer-based vs. metallic-based bioresorbable stents.* Journal of Thoracic Disease, 2017. **9**: p. S923-S934.
22. Fischell, T.A., et al., *Integrated Stent Delivery System: A Next Generation of Stent Delivery and Drug-Eluting Stent.* Cardiovascular Revascularization Medicine, 2020. **21**(2): p. 205-212.
23. Nakka, K., et al., *An overview of the design, development and applications of biodegradable stents.* Drug Delivery Letters, 2020. **10**(1): p. 2-13.
24. Thostenson, E.T., Z. Ren, and T.W. Chou, *Advances in the science and technology of carbon nanotubes and their composites: A review.* Composites Science and Technology, 2001. **61**(13): p. 1899-1912.
25. Baddour, C.E., et al., *A simple thermal CVD method for carbon nanotube synthesis on stainless steel 304 without the addition of an external catalyst.* Carbon, 2009. **47**(1): p. 313-318.
26. He, H., et al., *Carbon nanotubes: Applications in pharmacy and medicine.* BioMed Research International, 2013. **2013**.
27. Digge, M.S., R.S. Moon, and S.G. Gattani, *Application of carbon nanotubes in drug delivery: A review.* International Journal of PharmTech Research, 2012. **4**(2): p. 839-847.
28. Bhaskar, A.K., V.N. Deshmukh, and L. Prajapati, *Carbon nanotube as a drug delivery system: A reveiw.* International Journal of Pharmacy and Technology, 2013. **5**(2): p. 2695-2711.
29. He, H., et al., *Carbon nanotubes used as nanocarriers in drug and biomolecule delivery*, in *Drug Delivery Approaches and Nanosystems: Volume 1: Novel Drug Carriers*. 2017. p. 163-212.
30. Chakoli, A.N. and M. Sadeghzadeh, *Recent trends in biomedical and pharmaceutical industry due to engineered nanomaterials*, in *Handbook of Nanomaterials for Industrial Applications*. 2018. p. 499-519.

31. Das, M.K. and A. Sarma, *Carbon nanotubes and drug targets*, in *Frontiers in Drug Design and Discovery*. 2018. p. 176-202.
32. Huan, Y., et al., *Acrylic acid grafted-multi-walled carbon nanotubes and their high-efficiency adsorption of methylene blue.* Journal of Materials Science, 2020. **55**(11): p. 4656-4670.
33. Resende, M.M., et al., *Estimation of mass transfer parameters in a Taylor-Couette-Poiseuille heterogeneous reactor.* Brazilian Journal of Chemical Engineering, 2004. **21**(2): p. 175-184.
34. Frattolin, J., et al., *Development of a Novel Biodegradable Metallic Stent Based on Microgalvanic Effect.* Annals of Biomedical Engineering, 2016. **44**(2): p. 404-418.
35. Zhuo, C., et al., *Oxidative heat treatment of 316L stainless steel for effective catalytic growth of carbon nanotubes.* Applied Surface Science, 2014. **313**: p. 227-236.
36. Selen, V., et al., *Synthesized multi-walled carbon nanotubes as a potential adsorbent for the removal of methylene blue dye: kinetics, isotherms, and thermodynamics.* Desalination and Water Treatment, 2016. **57**(19): p. 8826-8838.